MEF2C regulates NK cell effector functions through control of lipid metabolism

Joey H. Li [1,2,3], Adalia Zhou[1], Cassidy D. Lee [1,2,3], Siya N. Shah[1], Jeong Hyun Ji [1,2], Vignesh Senthilkumar [1], Eddie T. Padilla [1,2], Andréa B. Ball [4], Qinyan Feng[1], Christian G. Bustillos[1,2], Luke Riggan[1,2], Alain Greige [5], Ajit S. Divakaruni[4], Fran Annese[6], Jessica Cooley-Coleman [6], Steven A. Skinner[6], Christopher W. Cowan[5] & Timothy E. O'Sullivan [1,2] ✉

Natural killer (NK) cells are a critical first line of defense against viral infection. Rare mutations in a small subset of transcription factors can result in decreased NK cell numbers and function in humans, with an associated increased susceptibility to viral infection. However, our understanding of the specific transcription factors governing mature human NK cell function is limited. Here we use a non-viral CRISPR–Cas9 knockout screen targeting genes encoding 31 transcription factors differentially expressed during human NK cell development. We identify myocyte enhancer factor 2C (MEF2C) as a master regulator of human NK cell functionality ex vivo. MEF2C-haploinsufficient patients and mice displayed defects in NK cell development and effector function, with an increased susceptibility to viral infection. Mechanistically, MEF2C was required for an interleukin (IL)-2- and IL-15-mediated increase in lipid content through regulation of sterol regulatory element-binding protein (SREBP) pathways. Supplementation with oleic acid restored MEF2C-deficient and MEF2C-haploinsufficient patient NK cell cytotoxic function. Therefore, MEF2C is a critical orchestrator of NK cell antiviral immunity by regulating SREBP-mediated lipid metabolism.

NK cells play a critical role during the early defense against viral infection via direct cytotoxicity against infected cells as well as the production of inflammatory cytokines such as interferon (IFN)-γ[1]. This is highlighted by the increased susceptibility to viruses displayed by NK cell-deficient individuals, often leading to premature death due to disseminated viral infection[2–7]. In the initial stages of viral infection, NK cells are exposed to a rich milieu of activating signals including pro-inflammatory cytokines secreted by local myeloid cells as well as direct ligation of activating receptors[1]. These signals result in transcriptional and epigenetic changes driving a dramatic burst of proliferation, production of effector molecules and heightened metabolic activity, enabling activated NK cells to deliver a rapid and potent antiviral response.

In humans, peripheral NK cells are developmentally stratified by differential expression of the markers CD56, CD16 and CD57 (refs. 8,9). Developmental subsets of human NK cells are functionally distinct, as CD56[bri]CD16^{−} cells produce more IFN-γ and display lower cytotoxicity than CD56^{dim}CD16^{+} cells. CD56^{dim}CD16^{+}CD57^{+} cells present the most mature receptor repertoire and the greatest cytolytic activity, in addition to displaying the greatest sensitivity to CD16 receptor activation[10,11]. Substantial transcriptional and epigenetic reprogramming occurs for NK cells to transition between these functionally distinct

[1]Department of Microbiology, Immunology and Molecular Genetics, David Geffen School of Medicine at UCLA, Los Angeles, CA, USA. [2]Molecular Biology Institute, University of California, Los Angeles, Los Angeles, CA, USA. [3]David Geffen School of Medicine at UCLA, Los Angeles, CA, USA. [4]Department of Molecular and Medical Pharmacology, David Geffen School of Medicine at UCLA, Los Angeles, CA, USA. [5]Department of Neuroscience, Medical University of South Carolina, Charleston, SC, USA. [6]Greenwood Genetic Center, Greenwood, SC, USA. ✉e-mail: tosullivan@mednet.ucla.edu

developmental stages[12]. Transcription factors such as EOMES, ETS1, T-BET, NFIL3 and ID2 are well characterized as regulators of NK cell development and effector function after activation[13–18]. For example, ETS1 drives the expression of T-BET, ID2 and activating receptors to promote effector function[13]. Understanding the transcriptional regulation of human NK cell function is clinically important, as multiple human NK cell deficiencies are caused by mutations in genes encoding transcription factors (*BCL11B*, *GATA2*) owing to their pleiotropic roles in gene regulation[2,3,19]. While mechanistic studies identifying transcription factors important for NK cell antiviral function are largely performed in mice, recent studies suggest that the transcriptional changes that are induced in mouse and human NK cells upon cytokine activation are largely species specific[20]. Therefore, a direct examination of transcription factor functions in primary human NK cells would facilitate the discovery of gene regulatory networks important for enhancing NK cell function in the clinic.

To identify transcription factors that control human NK cell function, we developed a targeted non-viral CRISPR–Cas9 ribonucleoprotein (cRNP)-based screening approach in primary human peripheral blood mononuclear cell (PBMC)-derived NK cells to evaluate the role of developmentally regulated transcription factors in positive or negative regulation of effector function[21,22]. Of 31 genes screened, *MEF2C* encoded the sole transcription factor broadly required for human NK cell homeostasis, cytokine production and cytotoxicity. MEF2C haploinsufficiency in both human patients and mice resulted in defective peripheral NK cell development, effector function and protection against viral infection. Mechanistically, MEF2C was induced by IL-15 signaling to increase neutral lipid content through SREBP signaling. Loss of MEF2C lowered intracellular lipid content and uptake through decreased low-density lipoprotein receptor (LDLR) levels, and supplementation with oleic acid restored the cytotoxic function of MEF2C-deficient NK cells. Thus, we identify MEF2C as a transcriptional regulator of NK cell effector function via the regulation of cytokine-activated lipid metabolic reprogramming and characterize a functional NK cell defect associated with MEF2C haploinsufficiency in humans.

Results

MEF2C is a critical regulator of human NK cell effector function

Previous studies indicate that the transcriptional responses of activated mouse and human NK cells are distinct between species, suggesting that gene regulatory networks identified in mice may not translate to human immunity[20]. We therefore sought to identify transcription factors required for primary human NK cell effector function. We referenced previously published multiomic datasets of peripheral human NK subsets (CD56[bri], CD56^{dim}CD57^{–} and CD56^{dim}CD57^{+}) sorted by flow cytometry, in which combined assay for transposase-accessible chromatin with sequencing motif analysis, histone H3 lysine 27 monoacetylation chromatin immunoprecipitation followed by sequencing and RNA sequencing (RNA-seq) identified 36 transcription factors for which binding sites were enriched in subset-specific putative enhancer regions and were differentially expressed between NK cell subsets[23]. For each of the 36 transcription factors, we tested four distinct single-guide RNAs (sgRNAs) to examine which genes were efficiently edited by cRNP editing. This yielded a final set of 31 transcription factor genes that could be edited with high efficiency in primary human NK cells (Extended Data Fig. 1a)[23]. As differential expression of CD56 and CD16 distinguishes immature cytokine-producing CD56[bri]CD16^{–} cells from mature cytotoxic CD56^{dim}CD16^{+} cells[8,10], we reasoned that these transcription factors may be natural regulators of inflammatory or cytotoxic human NK cell function. To directly test the role of these genes in human NK cell effector function, we performed a targeted knockout screen using cRNP editing of primary NK cells isolated from healthy human donor PBMCs[21,22] (Extended Data Fig. 1b). cRNP-edited NK cells

were evaluated for viable cell numbers, IFN-γ production in response to cytokine stimulation and killing of target cells. Of 31 candidates, we identified 11 positive regulators of NK cell function and ten negative or mixed regulators (Fig. 1a). These included transcription factors previously reported in the literature to positively regulate mouse NK cell function such as those encoded by *TCF7*, *MYC* and *ZEB2* (refs. 24–26) (Fig. 1a and Extended Data Fig. 1c–e). We also identified transcription factor functions consistent with reported immune cell deficiency in patients such as the requirement for *RORC* for NK cell IFN-γ production[27] (Extended Data Fig. 1f). However, multiple positive regulators were new and had no prior recognized role in human NK cell function.

Of the 31 genes screened, we identified *MEF2C* as the sole gene required for all tested NK cell functions (Fig. 1a). CRISPR cRNP-mediated MEF2C loss was verified by immunoblot and Sanger sequencing (Extended Data Fig. 2a,b). Compared with *TRAC* cRNP-edited (*TRAC*[cRNP]) NK cells, we recovered lower numbers of viable *MEF2C*-edited (*MEF2C*[cRNP]) cells from the same donor after cRNP editing (Fig. 1b). While we observed a slight increase in apoptotic *MEF2C*[cRNP] NK cells, the absolute change was insufficient to account for the difference in total viable cells (Extended Data Fig. 2c). Furthermore, loss of MEF2C did not significantly alter the ratio of prosurvival BCL2 versus pro-apoptotic BIM proteins (Extended Data Fig. 2d). Rather, *MEF2C*[cRNP] NK cells displayed a marked proliferative defect evidenced by decreased CellTrace Violet (CTV) dilution and Ki-67 expression (Fig. 1c,d). When stimulated with IL-12, IL-18 or a combination of both cytokines, *MEF2C*[cRNP] NK cells produced less IFN-γ and tumor necrosis factor (TNF)-α (Fig. 1e,f). *MEF2C*[cRNP] NK cells were also less cytotoxic toward K562 and A375 target cells (Fig. 1g and Extended Data Fig. 2e). This killing defect was accompanied by decreased degranulation and lower expression of granzyme B (GzmB), although perforin expression was unaffected (Fig. 1h,i and Extended Data Fig. 2f). Together, these results indicate that MEF2C is a critical regulator of IL-2- and IL-15-activated human NK cell effector function and proliferation.

MEF2C-haploinsufficiency syndrome is associated with NK cell defects

To confirm whether disruption of MEF2C expression in humans impacts NK cell function, we studied peripheral blood NK cells from patients with MEF2C-haploinsufficiency syndrome (MCHS), a recently described neurological syndrome caused by point mutations or microdeletions involving *MEF2C*[28]. We identified two patients with MCHS between the ages of 4 and 8 years old with clinical characteristics consistent with previous reports (Extended Data Fig. 3a and Table 1). Patient 1 initially presented with developmental delay and was identified to have a de novo pathogenic c.638-2A>G intronic mutation upstream of exon 7 of *MEF2C* by whole-exome sequencing, thought to disrupt the splice acceptor site of intron 7 (Extended Data Fig. 3a). Patient 2 was found to bear a de novo pathogenic c.90G>T (p.K30N) mutation localized to the DNA-binding MCM1, agamous, deficiens and serum response factor (MADS) domain in MEF2C identified by an epilepsy gene panel (Extended Data Fig. 3a). Neither patient had notable neutropenia on the most recent complete blood count with differential. Patient 1 displayed normal lymphocyte frequencies and counts, while the second patient presented with normal lymphocyte frequencies but decreased absolute lymphocytes. Because MEF2C is predominantly expressed in B cells, monocytes and NK cells, we examined the B cell, T cell and monocyte compartments of both patients by flow cytometry and found no major changes in frequencies compared with control healthy donor peripheral blood samples (Extended Data Fig. 3b,c).

However, patient 1 bearing an intronic point mutation (c.638-2A>G) displayed lower frequencies of cytotoxic CD56^{dim}CD16^{+} NK cells than healthy controls accompanied by higher proportions of immature CD56[bri]CD16[–/int] cells (Fig. 2a,b). After 5 d of activation with IL-2 and IL-15 ex vivo, CD56^{dim}CD16^{+} patient-derived NK cells produced lower levels of IFN-γ when stimulated with IL-12 and displayed
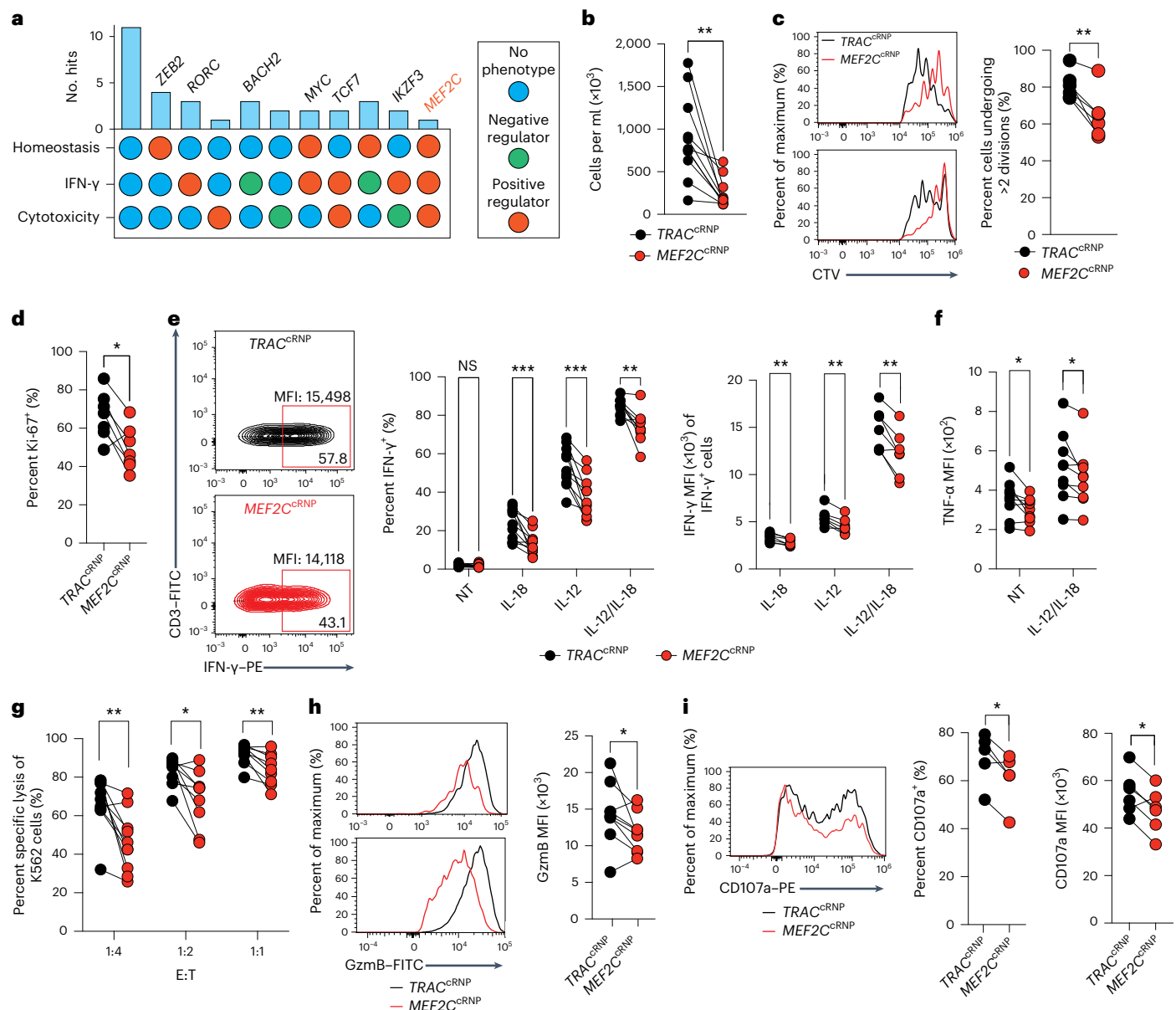
Fig. 1 | MEF2C is required for human NK cell proliferation and effector function. a, Overview of knockouts of transcription factors regulating NK cell function. **b**, Density of viable *TRAC*cRNP or *MEF2C*cRNP NK cells 6 d after cRNP editing, expanded with IL-2 and IL-15. **c**, Left: representative histograms showing dilution of CTV in *TRAC*cRNP or *MEF2C*cRNP NK cells on day 6 after cRNP editing. Right: frequency of cells undergoing more than two cell divisions. **d**, Frequency of Ki-67+ cells on day 6 after cRNP editing. **e**, Representative contour plots (left) and quantification of percent IFN-γ+ (center) and IFN-γ mean fluorescence intensity (MFI) of cytokine-producing cells (right) of *TRAC*cRNP or *MEF2C*cRNP NK cells after 16 h of stimulation with IL-2, IL-15, K562 cells and IL-12 and/or IL-18. NS, not significant; NT, no treatment. **f**, TNF-α MFI of NK cells stimulated for 16 h with IL-2, IL-15, K562 cells, IL-12 and IL-18. **g**, Specific lysis of K562 cells by edited NK cells after 16 h of co-culture with IL-2 and IL-15 at the indicated effector:target

(E:T) ratios. **h**, Representative histograms (left) and quantification (right) of GzmB expression in edited NK cells. **i**, Representative histogram (left) and quantification (right) of CD107a expression in edited NK cells cultured for 4 h with IL-2, IL-15, K562 cells, brefeldin A and monensin in the presence of anti-CD107a–PE antibody. **c**–**f**,**h**,**i**, Gated on CD56+CD3− cells. Data are representative of *n* = 6–11 independent donors presented as individual paired donors and are shown as mean ± s.e.m. *P < 0.05, **P < 0.01, ***P < 0.001 by two-sided paired *t*-test. Specific *P* values are as follows. For **b**, 0.0012. For **c**, 0.0056. For **d**, 0.0177. For **e**, percent IFN-γ+, NT (0.8166), IL-18 (0.0018), IL-12 (0.0003), IL-12 and IL-18 (0.0042); IFN-γ MFI, IL-18 (0.0019), IL-12 (0.0033), IL-12 and IL-18 (0.0032). For **f**, NT, 0.0262; IL-12 and IL-18, 0.0333. For **g**, 1:4, 0.0031; 1:2, 0.0120; 1:1, 0.0041. For **h**, 0.0490. For **i**, percent CD107a+, 0.0250; CD107a MFI, 0.0290.

moderately lower cytotoxicity against K562 target cells than healthy controls (Fig. 2c,d). Defects in cytokine production were restricted to the CD56dim population, as MCHS patient total or CD56bri NK cells produced similar amounts of IFN-γ as healthy controls, consistent with MEF2C being most highly expressed in CD56dim rather than CD56bri NK cells (Extended Data Fig. 3d,e). Clinically, this patient reported a history of recurrent otitis media. As MEF2C relies on DNA binding for transcriptional activator activity, we next examined NK cells from

patient 2 bearing a c.90G>T (p.K30N) disruption to the DNA-binding MADS domain (Extended Data Fig. 3a). This patient displayed an even more striking over-representation of CD56briCD16−/int cells and decreased numbers of CD56dimCD16+ NK cells (Fig. 2a,b). Functional testing of patient-derived NK cells revealed profound defects in inflammatory cytokine production from the CD56dim population as well as cytotoxicity, although cytokine production from CD56bri NK cells again remained intact (Fig. 2c,d and Extended Data Fig. 3d). Clinical

Table 1 | MCHS patient clinical features

Patient	1	2
MEF2C mutation	c.638-2A>G, heterozygous, de novo	c.90G>T (p.Lys30Asn), heterozygous, de novo
Sex	Male	Female
Clinical findings		
Seizures	–, but abnormal EEGs	+
Global developmental delay	+	+
Speech	Absent	Absent
Tremors/tremulous	–	–
Hypotonia	+	+
Brain MRI	Normal	Abnormal
Abnormalities noted	–	Asymmetric appearance of hippocampi, asymmetric enlargement of temporal horn of left lateral ventricle
Repetitive movements	+	–
Breathing abnormalities	–	+
Sleeping difficulties	+	–
Social abnormalities	+	+
Autism spectrum disorder	+	–
Immunologic findings		
Recurrent infections	+, ear infections requiring tympanostomy tubes	+, viral URI and ear infections
CBC	Normal	Decreased absolute lymphocyte numbers

EEG, electroencephalogram; MRI, magnetic resonance imaging; URI, upper respiratory infection; CBC, complete blood count.

findings revealed a history of severe and recurrent viral infections, suggestive of substantial immune dysfunction. While we observed no major disruptions of perforin expression in MCHS patient NK cells after 5 d of expansion with IL-2 and IL-15, MCHS patient NK cells displayed defective GzmB expression specifically in CD16^{int} and CD56^{dim}CD16$^+$ cells (Extended Data Fig. 3f,g). Consistent with the more pronounced defect in cytotoxicity seen in patient 2 bearing a MADS domain point mutation, GzmB production in CD56^{dim}CD16$^+$ cells from patient 2 was greatly reduced compared with that in healthy donor cells or cells from patient 1 (Extended Data Fig. 3h). These results indicate that germline MEF2C haploinsufficiency in humans is associated with developmental and functional defects preferentially impacting the mature CD56^{dim}CD16$^+$ NK cell subset.

As patients with MCHS bear germline *MEF2C* mutations in all somatic cells, we examined whether a cell-intrinsic point mutation in *MEF2C* in healthy donor-derived NK cells was sufficient to recapitulate the functional defects seen in MCHS patient-derived NK cells. We generated primary human NK cells bearing an intronic point mutation (c.1472+3A>G) in *MEF2C* via an sgRNA-targeted Cas9 adenine base editor (ABE8e) (Extended Data Fig. 3i). Efficient base editing was confirmed by Sanger sequencing (Extended Data Fig. 3j). Compared with electroporation of adenine base editor mRNA alone, the introduction of a *MEF2C* point mutation was sufficient to impair proliferation, cytotoxicity and cytokine production in healthy donor-derived human NK cells (Fig. 2e–h). Thus, NK cell-intrinsic

point mutations in MEF2C are sufficient to impair healthy mature human NK cell effector function.

MEF2C is required for antiviral immunity

Mef2c$^{+/-}$ mouse models have been shown to faithfully recapitulate the neurological aspects of MCHS, as homozygous deficiency in MEF2C is embryonic lethal[29,30]. Therefore, we generated mixed bone marrow chimeric (mBMC) mice engrafted with a 1:1 mixture of congenically distinct CD45.1 wild-type (WT) and CD45.2 *Mef2c$^{+/-}$* bone marrow to examine the effects of a clinically relevant degree of MEF2C deficiency on NK cell development and effector function (Extended Data Fig. 4a). After 4 weeks, *Mef2c$^{+/-}$* bone marrow-derived NK cells made up a smaller proportion of peripheral NK cells than WT (Extended Data Fig. 4b). We observed an increase in immature CD27$^+$CD11b$^+$ NK cells accompanied by a significant decrease in mature CD27$^-$CD11b$^+$ NK cells derived from *Mef2c$^{+/-}$* bone marrow in the periphery, mirroring the developmental block observed in MCHS patient NK cells (Extended Data Fig. 4c and Fig. 2a,b). Functionally, *Mef2c$^{+/-}$* NK cells produced less IFN-γ when stimulated ex vivo with IL-12 or IL-18 and displayed impaired degranulation upon anti-Ly49H activating receptor ligation ex vivo (Fig. 3a,b). Defective IFN-γ production was restricted to the mature CD27$^-$CD11b$^+$ subset of peripheral NK cells (Extended Data Fig. 4d,e), similar to the CD56^{dim}-restricted IFN-γ production defect observed in patients with MCHS (Extended Data Fig. 3d).

To determine whether functional defects in *Mef2c$^{+/-}$* NK cells were sufficient to confer increased susceptibility to viral infection in vivo, we generated single bone marrow chimeric (sBMC) mice engrafted with either WT or *Mef2c$^{+/-}$* bone marrow (Extended Data Fig. 4a). Upon viral challenge with a sublethal dose of mouse cytomegalovirus (MCMV), *Mef2c$^{+/-}$* sBMC mice lost more weight and succumbed more quickly to infection (Fig. 3c,d). Notably, mice died within the first 5 d of infection. While T cells are initially dispensable in MCMV infections, NK cells are required for immune protection early on, suggesting that the early mortality of *Mef2c$^{+/-}$* mice was likely attributable to a defect in the initial NK cell response[31,32]. We next infected WT:*Mef2c$^{+/-}$* mBMC mice to evaluate NK cell effector function in an internally controlled environment (Extended Data Fig. 4a). On day 1.5 after MCMV infection, *Mef2c$^{+/-}$* bone marrow-derived NK cells produced lower amounts of IFN-γ and GzmB than WT bone marrow-derived NK cells in the same host (Fig. 3e,f). As seen ex vivo, IFN-γ production defects were most significant in the mature CD27$^-$CD11b$^+$ subset of peripheral NK cells responding to MCMV infection (Extended Data Fig. 4f). To examine whether MEF2C haploinsufficiency impacted clonal expansion during MCMV infection, we co-adoptively transferred WT and *Mef2c$^{+/-}$* Ly49H$^+$ NK cells into *Klra8$^{-/-}$* hosts to clonally proliferate in response to MCMV infection (Extended Data Fig. 4g). At the peak of NK cell expansion on day 7 after infection, *Mef2c$^{+/-}$* NK cells displayed markedly impaired expansion compared with cotransferred WT cells in multiple organs (Fig. 3g).

To test whether MEF2C is required for mature NK cell proliferation independent of the role of MEF2C in NK cell development in vivo, we ablated *Mef2c* expression in mature splenic mouse NK cells using cRNP electroporation (*Mef2c^{cRNP}*) and adoptively transferred a mixture of congenically distinct *Mef2c^{cRNP}* and control *Rosa26^{cRNP}* Ly49H$^+$ NK cells at a 1:1 ratio to *Klra8$^{-/-}$* hosts and infected them with MCMV immediately after transfer (Extended Data Fig. 4h). On day 7 after infection, the proportion of Ly49H$^+$KLRG1$^+$ *Mef2c^{cRNP}* NK cells was lower than that of co-adoptively transferred controls in the peripheral blood of recipient mice (Extended Data Fig. 4i). Similar to human NK cells, *Mef2c^{cRNP}* NK cells displayed deficient production of IFN-γ in response to activating cytokines as well as impaired cytotoxicity against β$_2$-microglobulin (β$_2$M)-deficient MC38 tumor targets ex vivo (Extended Data Fig. 4j,k). These findings demonstrate that MEF2C is required for both ex vivo and in vivo antiviral activity of mouse NK cells, and MEF2C haploinsufficiency in the hematopoietic compartment of mice is sufficient to increase morbidity and mortality during viral infection.
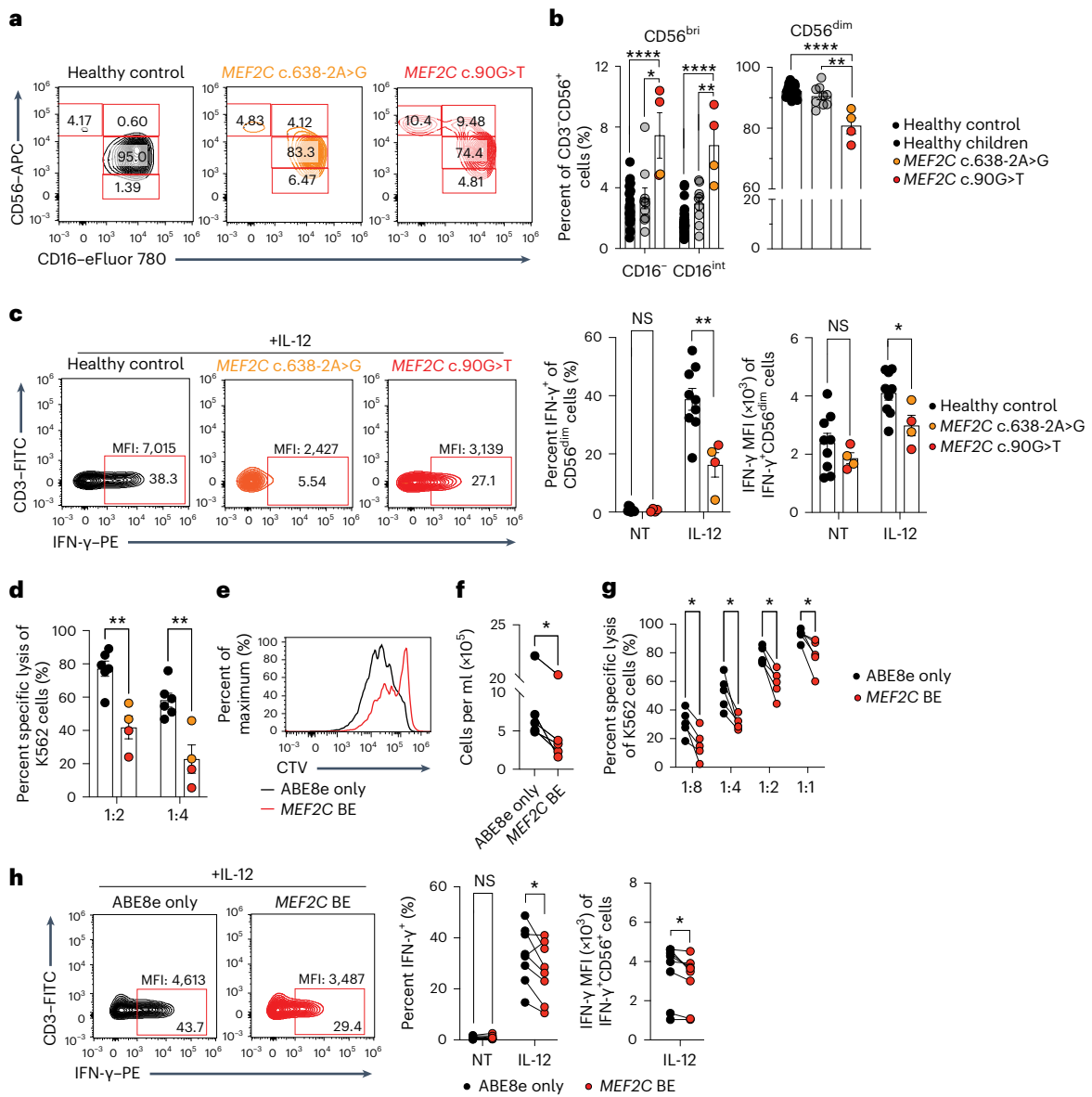
Fig. 2 | Patients with MCHS present with a functional NK cell deficiency.
a,b, Representative contour plots (**a**) and quantification (**b**) showing NK cell maturation in freshly isolated PBMCs from healthy donor controls or patients with MCHS. **c**, Representative contour plots (left) and quantification of percent IFN-γ⁺ cells (center) and IFN-γ MFI of cytokine-producing cells (right) of CD56^dim healthy donor control or patient NK cells stimulated for 16 h with IL-2, IL-15, K562 cells and IL-12 after 5 d of expansion with IL-2 and IL-15. **d**, Specific lysis of K562 cells by healthy donor control or patient NK cells co-cultured for 16 h with K562 cells, IL-2 and IL-15 after 5 d of expansion with IL-2 and IL-15. **e**, Representative histogram of CTV dilution in control or base-edited (BE) human NK cells 6 d after base editing. **f**, Density of viable control or base-edited NK cells 6 d after base editing. **g**, Specific lysis of K562 cells by control or base-edited NK cells co-cultured as in **d**. **h**, Representative contour plots (left) and quantification of percent IFN-γ⁺ cells (center) and IFN-γ MFI of cytokine-producing cells (right) of

control or base-edited NK cells stimulated as in **c**. **a**,**b**,**e**,**f**,**h**, Gated on CD56⁺CD3⁻ cells. **c**, Gated on CD56^dimCD16⁺CD56⁺CD3⁻ cells. Data represent mean ± s.e.m. or individual paired donors. Data are representative of $n = 14$ (**b**), $n = 6$ (**c**,**d**) and $n = 7$ (**e**–**h**) independent healthy donors alongside $n = 2$ patients with MCHS, each sampled two independent times where applicable. *$P < 0.05$ by two-sided paired t-test or Student's t-test. Specific P values are as follows. For **b**, CD56^briCD16⁻ control versus patient, <0.0001; healthy children versus patient, 0.0138; CD56^briCD16^int control versus patient, <0.0001; healthy children versus patient, 0.0027; CD56^dim control versus patient, <0.0001; healthy children versus patient, 0.0019. For **c**, percent IFN-γ⁺, NT (0.6644), IL-12 (0.0044); IFN-γ MFI, NT (0.3327), IL-12 (0.0276). For **d**, 1:2, 0.0020; 1:4, 0.0031. For **f**, 0.0173. For **g**, 1:8, 0.0133; 1:4, 0.0146; 1:2, 0.0052; 1:1, 0.021. For **h**, percent IFN-γ⁺, NT (0.5197), IL-12 (0.0323); IFN-γ MFI (0·0177).

MEF2C is required for IL-15- and mTOR-induced metabolic reprogramming

Early during viral infection, activating cytokines in the local environment such as IL-2 and IL-15 stimulate increased NK cell proliferation and effector function[1]. We therefore hypothesized that MEF2C may be induced by cytokine stimulation to support enhanced effector function. We assessed MEF2C protein expression in healthy donor human NK cells stimulated with IL-2 and IL-15 for 72 h ex vivo compared

with that of freshly isolated cells and observed marked induction of MEF2C protein (Fig. 4a). As IL-2 and IL-15 signal through the shared IL-2Rβ and common γc receptor components, we pharmacologically inhibited signaling pathways downstream of these shared receptors. While inhibition of the mitogen-activated protein kinase (MAPK) pathway did not impact MEF2C expression, signal transducer and activator of transcription (STAT)5 was required for the IL-2- and IL-15-dependent increase in MEF2C protein levels (Fig. 4b). MEF2C induction by IL-2
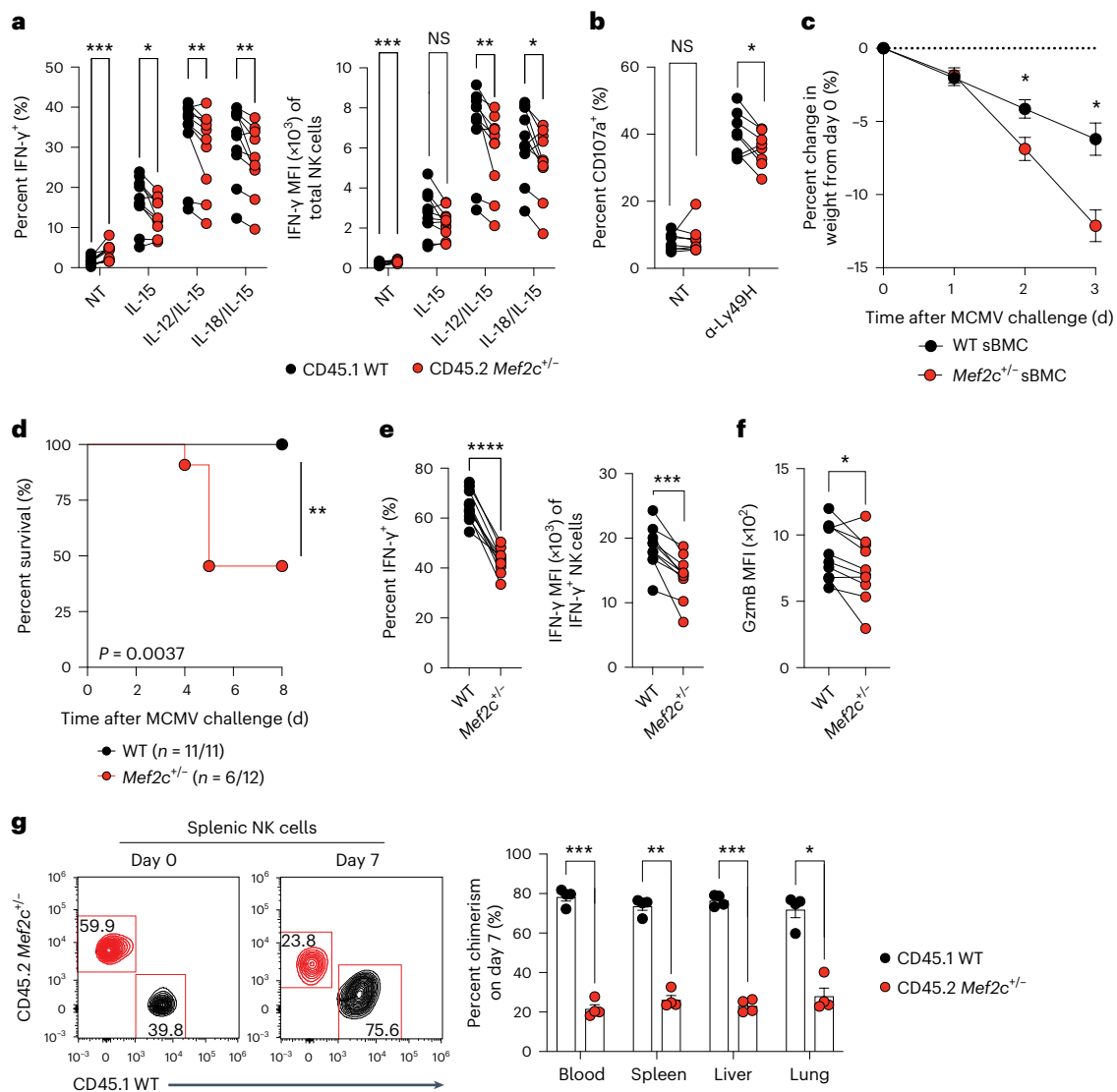
Fig. 3 | MEF2C haploinsufficiency disrupts antiviral immunity. a, Percent IFN-γ⁺ (left) and IFN-γ MFI of total NK cells (right) of WT or *Mef2c*⁺/⁻ splenic NK cells stimulated ex vivo for 4 h with IL-15, brefeldin A, monensin, IL-12 and/or IL-18. **b**, Percent CD107a⁺ WT or *Mef2c*⁺/⁻ bone marrow-derived splenic NK cells stimulated ex vivo with anti-Ly49H antibody for 4 h with IL-15, brefeldin A and monensin. **c**, Percent change in body weight from day 0 of WT or *Mef2c*⁺/⁻ sBMC mice infected with a sublethal dose of MCMV. **d**, Kaplan–Meier survival curves of WT or *Mef2c*⁺/⁻ sBMC mice infected with a sublethal dose of MCMV. **e**, Percent IFN-γ values (left) and IFN-γ MFI of cytokine-producing cells (right) of WT or *Mef2c*⁺/⁻ splenic NK cells in WT:*Mef2c*⁺/⁻ mBMC mice on day 1.5 after MCMV infection. **f**, GzmB MFI of WT or *Mef2c*⁺/⁻ bone marrow-derived splenic NK cells in WT:*Mef2c*⁺/⁻ mBMC mice on day 1.5 after MCMV infection. **g**, Representative contour plots showing splenic NK cell ratios on days 0 and 7 (left) and quantification on day 7 (right) in peripheral organs of WT or *Mef2c*⁺/⁻ NK cells cotransferred into male *Klra8*⁻/⁻ hosts and infected with MCMV. **a,b**, Gated on CD3⁻TCR-β⁻NK1.1⁺ cells. **e–g**, Gated on CD3⁻TCR-β⁻NK1.1⁺Ly49H⁺KLRG1⁺ cells. Data are representative of at least two independent experiments. Data represent mean ± s.e.m. or paired WT and *Mef2c*⁺/⁻ bone marrow-derived cells from the same mBMC mouse where applicable. Data are representative of *n* = 11 mice (**a,b**), *n* = 23 mice (**c,d**), *n* = 10 mice (**e,f**) and *n* = 4 (**g**) mice. *P < 0.05, **P < 0.01, ***P < 0.001, ****P < 0.0001 by two-sided paired *t*-test (**a,b,e–g**), two-sided Student's *t*-test (**c**) or Mantel–Cox test (**d**). Specific *P* values are as follows. For **a**, percent IFN-γ⁺, NT (0.0008), IL-15 (0.0109), IL-12 and IL-15 (0.0074), IL-18 and IL-15 (0.0074); IFN-γ MFI, NT (0.0003), IL-15 (0.0723), IL-12 and IL-15 (0.0042), IL-18 and IL-15 (0.0167). For **b**, NT, 0.5830; Ly49H, 0.0408. For **c**, 0.0176, 0.0114. For **d**, 0.0037. For **e**, percent IFN-γ⁺, <0.0001; IFN-γ MFI, 0.0002. For **f**, 0.0138. For **g**, blood, 0.0009; spleen, 0.0016; liver, 0.0004; lung, 0.0125.

and IL-15 stimulation was also dependent on phosphoinositol-3-kinase (PI3K) and mammalian target of rapamycin (mTOR) complex 1 (mTORC1) activity, as inhibition of these pathways decreased MEF2C expression to unstimulated levels (Fig. 4c). In contrast, PI3K and mTORC1 signaling remained intact in MEF2C-deficient NK cells, as we observed no consistent changes in phosphorylation of AKT or ribosomal protein S6 across donors between *TRAC*ᶜᴿᴺᴾ and *MEF2C*ᶜᴿᴺᴾ cells (Fig. 4d), indicating that MEF2C was not upstream of these pathways. Furthermore, expression of the IL-2 and IL-15 receptor components CD25 (IL-2Rα) and CD122 (IL-2Rβ) were unaffected by MEF2C heterozygosity in both naive mouse NK cells and those at day 1.5 after MCMV infection as well as MEF2C

loss in cRNP-edited human NK cells (Extended Data Fig. 5a,b). Indeed, levels of phosphorylated STAT5 and STAT1 remained unchanged in *Mef2c*⁺/⁻ NK cells after MCMV infection, while IL-2- and IL-15-activated *TRAC*ᶜᴿᴺᴾ and *MEF2C*ᶜᴿᴺᴾ human NK cells displayed similar phosphorylated STAT5 levels (Extended Data Fig. 5c,d). These results suggest that the impaired effector function of NK cells after MEF2C loss is not likely due to defective cytokine receptor signaling.

Previous studies indicate that metabolic reprogramming is required for high levels of effector function in cytokine-treated NK cells[33]. IL-15 potently induces metabolic changes in NK cells via mTOR activation[34]. Considering the profound functional defects observed in
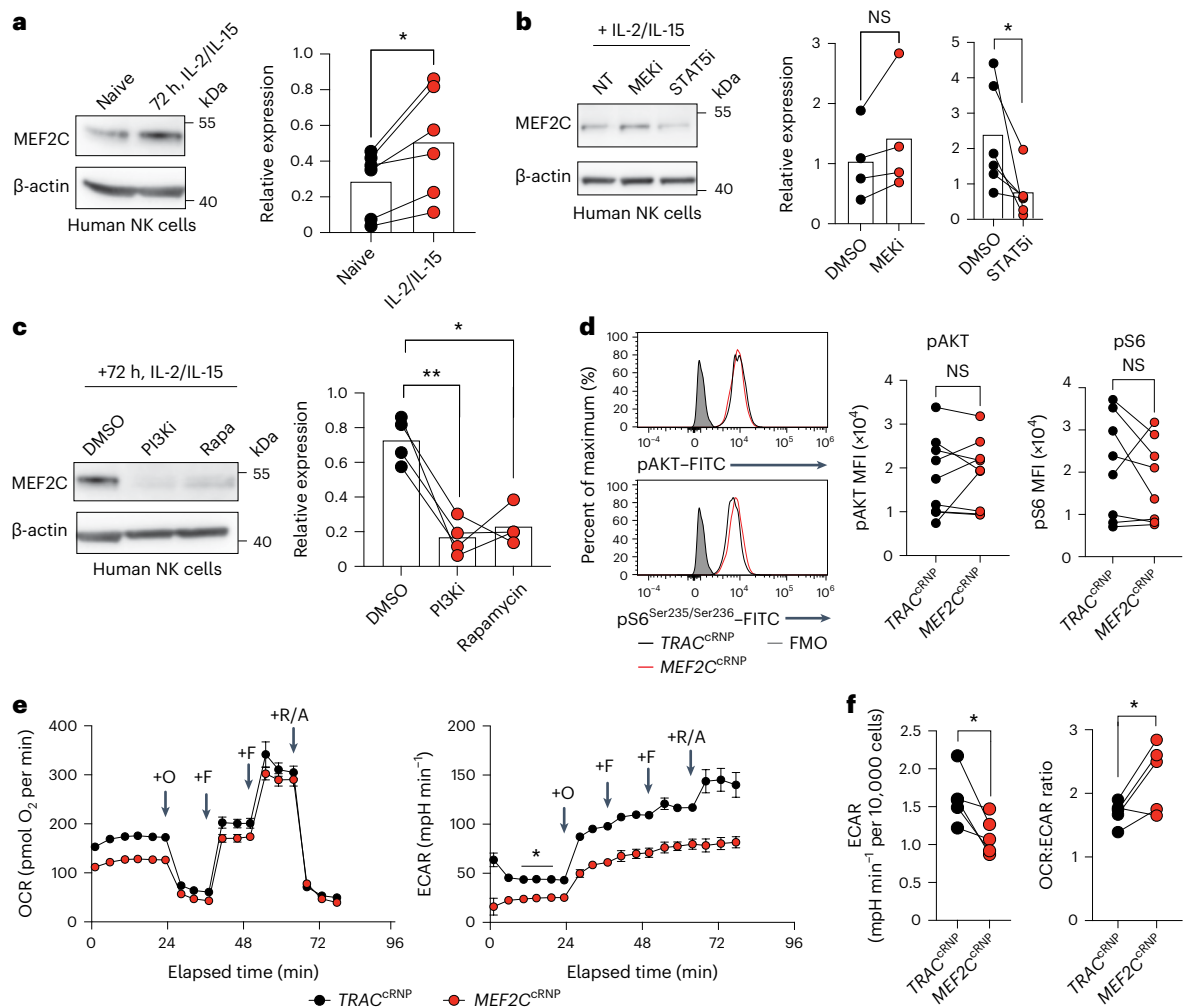
Fig. 4 | MEF2C is required for IL-15- and mTORC1-induced metabolic reprogramming. a, Immunoblot showing MEF2C and β-actin loading control protein levels in naive human NK cells or cells stimulated with IL-2 and IL-15 for 72 h (left) with quantification (right). **b**, Immunoblot showing MEF2C and β-actin loading control protein levels in human NK cells stimulated with IL-2 and IL-15 for 72 h alone or with the mitogen-activated protein kinase kinase (MEK) inhibitor (MEKi) AZD6244 (50 μM) or the STAT5 inhibitor (STAT5i) CAS 285986-31-4 (100 μM) (left) with quantification (right). DMSO, dimethylsulfoxide. **c**, Immunoblot showing MEF2C and β-actin loading control protein levels in human NK cells stimulated with IL-2 and IL-15 for 72 h alone or with the PI3K inhibitor (PI3Ki) LY294002 (50 μM) or the mTORC1 inhibitor rapamycin (rapa; 20 nM) (left) with quantification (right). **d**, Representative histograms (left)

and MFI of phosphorylated (p)AKT (center) and pS6 (right) in *TRAC*cRNP or *MEF2C*cRNP human NK cells 6 d after CRISPR editing. FMO, fluorescence minus one control. **e**, OCR and ECAR of *TRAC*cRNP and *MEF2C*cRNP NK cells measured by the Seahorse extracellular flux assay. O, oligomycin; F, carbonyl cyanide-*p*-trifluoromethoxyphenylhydrazone (FCCP); R/A, rotenone and antimycin A. **f**, Quantification of basal ECAR and the ratio of OCR to ECAR from **e**, normalized to the rate per 10,000 cells. Data represent mean ± s.e.m. of technical replicates (**e**) or $n = 6$ (**a**), $n = 4$ (MEK inhibitor) or $n = 6$ (STAT5 inhibitor) (**b**), $n = 5$ (**c**), $n = 8$ (**d**) or $n = 5$ (**e**,**f**) paired independent donors. *$P < 0.05$, **$P < 0.01$ by two-sided paired *t*-test. Specific *P* values are as follows. For **a**, 0.0164. For **b**, 0.0429. For **c**, DMSO versus PI3Ki, 0.0061; DMSO versus rapamycin, 0.0224. For **e**, 0.0327. For **f**, ECAR, 0.0327; OCR:ECAR, 0.0462.

our initial screen (Fig. 1), we hypothesized that MEF2C induction may broadly promote NK cell metabolic changes in response to cytokine stimulation and mTORC1 activation. Seahorse extracellular flux analysis of IL-2- and IL-15-activated *TRAC*cRNP and *MEF2C*cRNP NK cells revealed decreased extracellular acidification rate (ECAR) and an increased ratio of oxygen consumption rate (OCR) to ECAR in the absence of MEF2C (Fig. 4e,f). There was no significant difference in maximal OCR, suggesting that this metabolic shift was specific to adaptations resulting from cytokine activation (Extended Data Fig. 5e). These metabolic changes were confirmed across mature NK cell subsets by single-cell metabolic profiling using Single Cell ENergetic metabolism by profiling Translation inHibition (SCENITH), which revealed robust inhibition of translation by oligomycin treatment as well as decreased glycolytic capacity and increased dependence on oxidative phosphorylation for ATP production upon MEF2C loss (Extended Data Fig. 5f). While these trends were consistent across all NK cell developmental subsets, altered

metabolism was seen most significantly in the CD16+CD57− subset, suggesting that this subset is most dependent on MEF2C for maintaining metabolic fitness after cytokine activation (Extended Data Fig. 5g). Thus, MEF2C is required for mTORC1-mediated metabolic reprogramming upon IL-15 stimulation in mature peripheral human NK cells.

MEF2C mediates NK cell SREBP signaling and lipid metabolism
To interrogate the genes regulated by MEF2C that may control NK cell metabolism, we performed bulk transcriptomics in human and mouse CRISPR-edited NK cells. Upon MEF2C loss, expression of most differentially expressed genes (DEGs) was decreased in both human and mouse NK cells, suggesting that MEF2C primarily acts as a transcriptional activator in NK cells (Fig. 5a and Extended Data Fig. 6a). We observed a notable decrease in expression of genes associated with SREBP-mediated lipid metabolism in both species, where *SCD* and *Scd1* encoding stearoyl-CoA desaturase was one of the most significantly
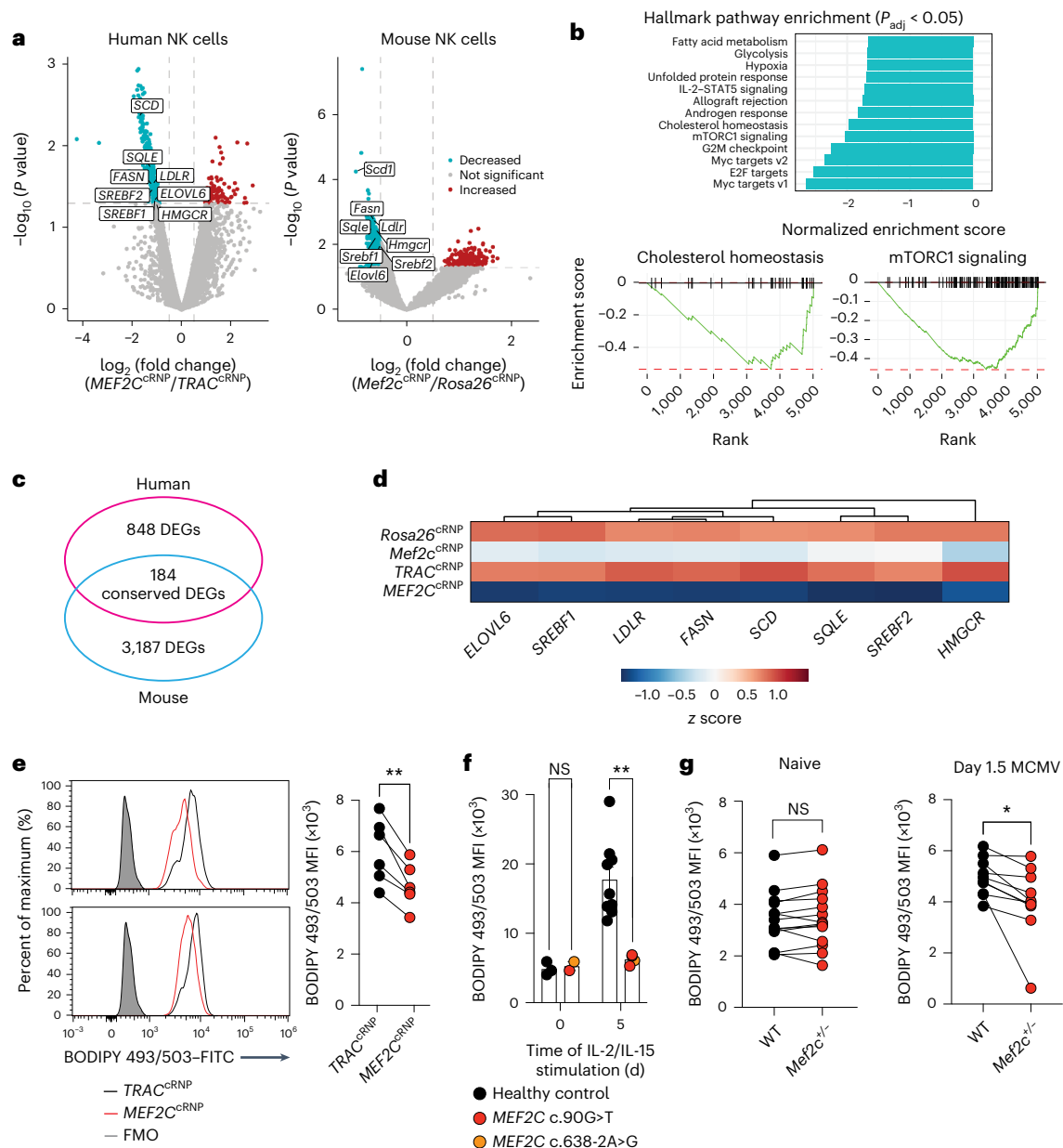
Fig. 5 | MEF2C promotes cytokine-activated SREBP signaling and increased lipid content in NK cells. a, Volcano plots displaying significant DEGs in cRNP-edited human (left) or mouse (right) NK cells compared with non-targeting controls with labeled genes of interest. For human NK cells, RNA samples were from paired $TRAC^{cRNP}$ and $MEF2C^{cRNP}$ NK cells from three independent donors. For mouse NK cells, RNA was extracted in triplicate from isolated NK cells from two mice pooled and edited with $Rosa26^{cRNP}$ or $Mef2c^{cRNP}$. **b**, GSEA of $MEF2C^{cRNP}$ human NK cells compared with the $TRAC^{cRNP}$ control. P_{adj}, adjusted P value. **c**, RNA-seq on human and mouse control and $MEF2C$- and $Mef2c$-knockout NK cells identified 184 conserved DEGs. **d**, Heatmap showing changes in gene expression of canonical SREBP pathway genes with hierarchical clustering of genes. **e**, Representative histograms (left) and MFI of BODIPY 493/503 staining (right) in $TRAC^{cRNP}$ or $MEF2C^{cRNP}$ NK cells on day 6 after cRNP editing and expansion with IL-2 and IL-15. **f**, MFI of BODIPY 493/503 in healthy control or MCHS patient NK cells immediately after isolation or after 5 d of expansion with IL-2 and IL-15. **g**, BODIPY 493/503 MFI of WT or $Mef2c^{+/-}$ bone marrow-derived splenic NK cells under uninfected conditions (left) or on day 1.5 after MCMV infection (right) in WT:$Mef2c^{+/-}$ mBMC mice. **e,f**, Gated on CD3⁻CD56⁺ cells. **g**, Gated on naive CD3⁻TCR-β⁻NK1.1⁺ or day 1.5 CD3⁻TCR-β⁻NK1.1⁺Ly49H⁺KLRG1⁺ cells. Data are representative of at least two independent experiments. Data represent mean ± s.e.m. or individual paired donors where applicable. Data are representative of n = 6 mice and n = 3 independent donors (**a**–**d**), n = 7 independent donors (**e**), n = 3–8 healthy donors and n = 2 patients with MCHS each sampled two independent times (**f**) and n = 11 naive and n = 10 MCMV-infected mice at day 1.5 (**g**). *P < 0.05, **P < 0.01 by two-sided paired t-test (**e,g**) or two-sided Student's t-test (**f**). Specific P values are as follows: 0.0026 (**e**); day 0 (0.7548), day 5 (0.0019) (**f**); naive (0.3860), day 1.5 (0.0190) (**g**).

downregulated genes in both mouse and human cRNP-edited cells (Fig. 5a). Indeed, gene set enrichment analysis (GSEA) performed on all DEGs in $MEF2C^{cRNP}$ human NK cells compared with $TRAC^{cRNP}$ controls revealed decreased expression of genes associated with fatty acid metabolism, cholesterol homeostasis, mTORC1 signaling and glycolysis pathways (Fig. 5b). We identified 184 DEGs conserved between species

regulated by MEF2C (Fig. 5c) and performed gene ontology analysis on this gene set to confirm GSEA findings. Gene ontology analysis showed that most pathways altered by MEF2C loss were related to mitosis and cell division, consistent with the defective proliferative phenotype we observed in multiple settings (Extended Data Fig. 6b). Exclusion of mitosis-associated pathways revealed enrichment in SREBP signaling,

lipid metabolism and glycolysis, in agreement with GSEA analysis. Gene ontology analysis also highlighted changes in hippocampal and substantia nigra brain development pathways reflective of the neurodevelopmental delays seen in patients with MCHS (Extended Data Fig. 6c). Indeed, genes associated with canonical SREBP signaling were downregulated in both MEF2C-deficient human and mouse NK cells (Fig. 5d and Extended Data Fig. 6d). Decreased *SREBF1* and *SCD* transcript expression were confirmed by quantitative PCR with reverse transcription (Extended Data Fig. 6e). Consistent with dysregulated lipid homeostasis upon MEF2C loss, we observed significantly decreased total neutral lipid content in IL-2- and IL-15-stimulated *MEF2C*cRNP NK cells by BODIPY 493/503 staining (Fig. 5e). While unstimulated healthy donor and MCHS patient-derived NK cells initially had similar lipid content, MCHS patient-derived NK cells displayed lower lipid levels after 5 d of IL-2 and IL-15 stimulation than healthy donor controls, suggesting that MEF2C is necessary for the cytokine-induced increase in lipid content in human NK cells (Fig. 5f). In vivo, while MCMV infection increased lipid content in both WT and *Mef2c*+/− mouse NK cells in mBMC mice (Extended Data Fig. 6f), *Mef2c*+/− cells increased lipid stores less than WT cells on day 1.5 after infection despite starting with similar lipid levels before infection (Fig. 5g). These findings highlight the key role of MEF2C in promoting SREBP-mediated lipid metabolism in cytokine-stimulated NK cells both in vitro and during in vivo viral infection.

Lipid supplementation restores MEF2C-deficient NK cell cytotoxicity

Intracellular lipid content can be modulated through lipid synthesis pathway activity or uptake of environmental lipids via receptors such as CD36 or LDLR[35]. IL-2- and IL-15-stimulated *MEF2C*cRNP NK cells displayed impaired lipid uptake evidenced by decreased BODIPY C12 uptake (Fig. 6a). Indeed, analysis of ex vivo cytokine-stimulated mouse and human NK cells revealed increased *LDLR* and *Ldlr* transcript expression upon stimulation with IL-2 and IL-15 (Fig. 6b). Splenic NK cells similarly increased *Ldlr* expression throughout the expansion phase of MCMV infection, reaching a peak in expression at day 7 after infection (Fig. 6c). Consistent with bulk transcriptomic findings in cRNP-edited cells (Fig. 5a), we observed markedly decreased LDLR protein levels upon cRNP-mediated MEF2C loss in healthy donor human NK cells (Fig. 6d,e). After stimulation with IL-2 and IL-15, MCHS patient-derived NK cells increased LDLR levels less than healthy donor NK cells (Fig. 6f). To evaluate the role of LDLR in maintaining human NK cell effector function, we ablated *LDLR* expression in healthy donor primary NK cells by cRNP electroporation and evaluated cytotoxicity and cytokine production of cRNP-edited cells. Loss of LDLR protein expression and decreased lipid content after cRNP editing was confirmed by flow cytometry (Extended Data Fig. 6g,h). *LDLR*cRNP NK cells phenocopied *MEF2C*cRNP NK cells, displaying lower production of IFN-γ as well as lower cytolytic activity against K562 targets than paired *TRAC*cRNP controls (Fig. 6g,h), suggesting that LDLR-mediated lipid uptake is required for optimal activated human NK cell function ex vivo.

SREBP proteins are key drivers of lipid metabolism in mammalian cells[36]. SREBP1 is a master activator of fatty acid synthesis, driving elongation and desaturation of the C16:0 fatty acid palmitate into C18:1 oleate via a C18:0 intermediate, stearate (Extended Data Fig. 6i). This process relies on the activity of fatty acid elongase 6 (encoded by *ELOVL6*) and stearoyl-CoA desaturase (encoded by *SCD*). Likewise, SREBP2 activation increases activity of sterol synthetic and uptake pathways. As we observed profoundly decreased expression of *ELOVL6*, *SCD*, *HMGCR* and *SQLE* and their mouse equivalents upon MEF2C loss in both human and mouse NK cells, we hypothesized that supplementation of NK cells with the lipid products of SREBP-mediated lipid synthesis may rescue MEF2C-deficient NK cell function. In cytokine-stimulated human NK cells, oleate but not cholesterol or palmitate supplementation increased cytotoxicity against K562 targets

(Fig. 6i). Oleate pretreatment was sufficient to restore the cytotoxicity of *MEF2C*cRNP NK cells to the levels of corresponding paired donor *TRAC*cRNP cells, consistent with *SCD* as one of the most significantly downregulated genes upon MEF2C loss (Figs. 6j and 5a). Notably, oleate treatment of IL-2- and IL-15-stimulated MCHS patient NK cells was sufficient to increase cytotoxicity to varying degrees. Lipid treatment of *MEF2C* c.638-2A>G patient NK cells markedly restored killing activity to near healthy adult donor levels, while supplementation of *MEF2C* c.90G>T patient NK cells only modestly improved cytotoxicity (Fig. 6k). Thus, we show that, upon cytokine activation, MEF2C links PI3K–AKT-induced mTORC1 activation and downstream lipid metabolism programs under the control of SREBPs to promote antiviral NK cell effector function (Extended Data Fig. 6i). Germline disruption of these programs controlled by MEF2C results in NK cell defects in patients with MCHS and *Mef2c*+/− mice, resulting in increased susceptibility to viral infection.

Discussion

While prior studies have applied pooled CRISPR cRNP screens to link genes to immune cell function in human T cells, monocytes and monocyte-derived dendritic cells, to our knowledge, our findings represent the first use of a non-viral targeted CRISPR cRNP screen in primary human NK cells. Our study highlights the utility of this approach to directly study gene function in human cells and reveal targets with both new cellular function and direct clinical relevance, identifying an unexpected NK cell defect associated with MCHS. Furthermore, we show that Cas9 base editing can also be used to validate cell-intrinsic functional effects of patient gene variants in healthy donor primary NK cells. Cas9 base editing has been used to study hematopoiesis and attribute pathogenicity to variants of unknown relevance in CD34+ hematopoietic stem progenitor cells in patients with clinically diagnosed disorders of hematopoiesis[37]. Therapeutically, adenine base editors have been used to correct pathogenic CD3δ severe combined immunodeficiency mutations in HPSCs and restore T cell development in a preclinical study[38]. Future applications of base editor-based functional validation of patient variants may be enhanced by computational prediction of variants most likely to disrupt protein structure, narrowing the range of variants requiring functional testing and potentially screening for new immune deficiencies[39].

MEF2C deficiency predominantly affects mature peripheral NK cell populations, displaying functional effects in CD56dimCD16+ MCHS patient NK cells and the corresponding CD27−CD11b+ mouse NK cell population. As this mature subset represents most peripheral NK cells in both species, defects in this population result in an overall decrease in NK cell function and increased susceptibility to viral infection observed in both mouse models and patients with MCHS, even with normal CD56bri NK cell activity. These findings are consistent with differential expression of *MEF2C* in NK cell subsets, highest in the CD56dimCD16+ population. As previous studies have found unique metabolic demands between the more inflammatory CD56bri versus cytotoxic CD56dim human NK cells, our results suggest that differential requirements for lipid metabolism may also exist between these subsets and deserve further investigation[40].

Our study also identifies MEF2C as a previously unidentified master transcription factor linking extracellular cytokine stimulation and mTORC1 activation to SREBP-mediated lipid homeostasis in NK cells. SREBP signaling is required for NK cell metabolic reprogramming in SREBP cleavage activating protein (SCAP)-deficient mouse models, which lack activation of both SREBP1 and SREBP2, although these studies focus on SREBP-mediated regulation of the citrate malate shuttle rather than lipid homeostasis[41]. Thus, these results support the critical role of SREBPs as key metabolic mediators in a broad array of immune populations including NK cells. While kinases such as S6 kinase downstream of mTORC1 have been suggested to be required for induction of glycolysis and SREBP activation in response to mitogenic
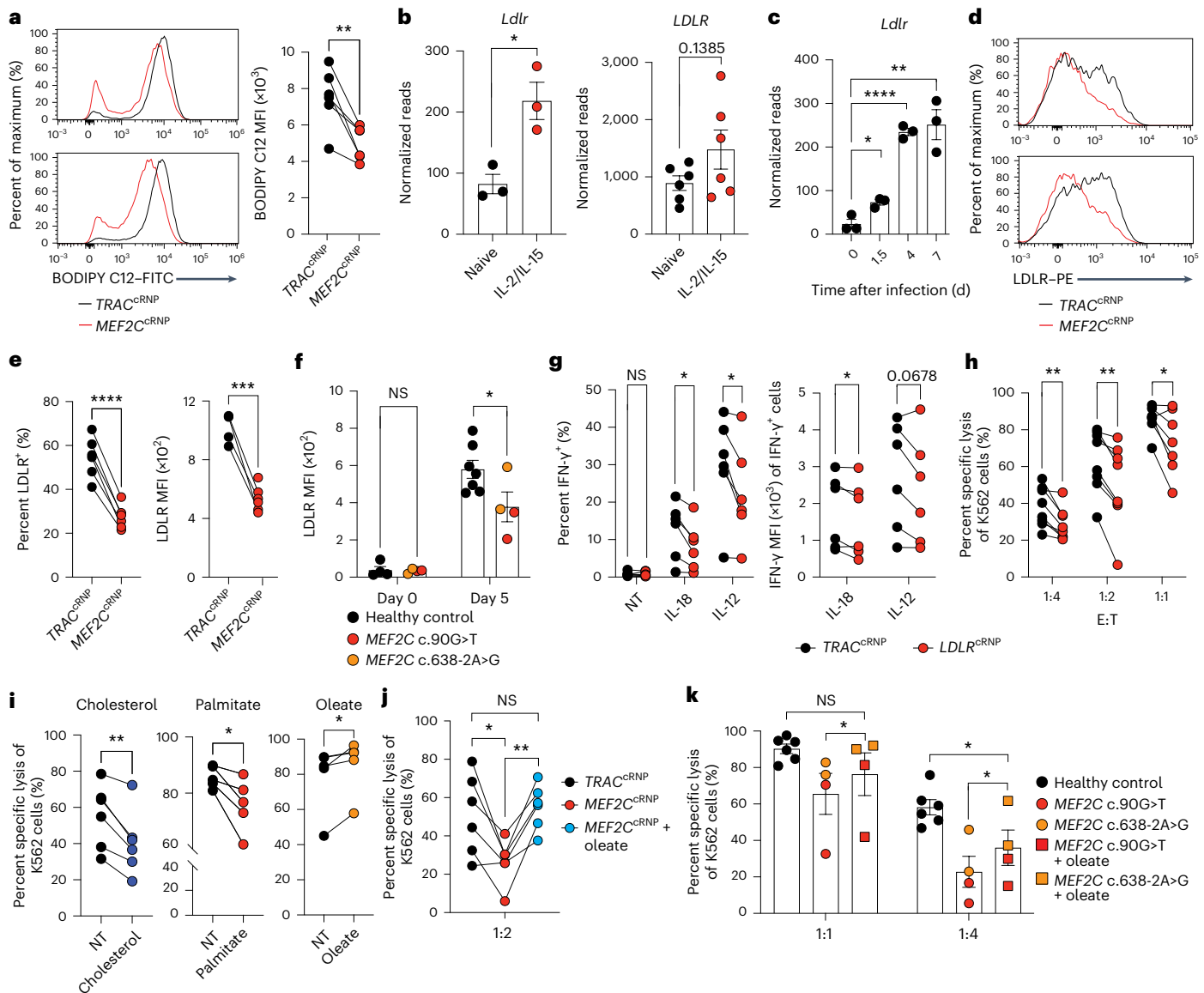
Fig. 6 | Fatty acid supplementation restores MEF2C-deficient NK cell cytotoxicity. a, Representative histograms (left) and MFI (right) of BODIPY C12 uptake in $TRAC^{cRNP}$ or $MEF2C^{cRNP}$ NK cells on day 6 after cRNP editing. **b**, $LDLR$ and $Ldlr$ transcript expression of naive or (3 h) IL-2- and IL-15-activated mouse (left) or human (right) NK cells. **c**, $Ldlr$ transcript expression of splenic NK cells after MCMV infection. **d,e**, Representative histograms (**d**) and percent $LDLR^+$ and LDLR MFI (**e**) of $TRAC^{cRNP}$ or $MEF2C^{cRNP}$ human NK cells 6 d after cRNP editing. **f**, LDLR MFI of naive or (5 d) IL-2- and IL-15-stimulated healthy donor or MCHS patient human NK cells. **g**, Quantification of percent IFN-γ⁺ (left) and IFN-γ MFI of cytokine-producing cells (right) of $TRAC^{cRNP}$ or $LDLR^{cRNP}$ NK cells after 16 h of stimulation with IL-2, IL-15, K562 cells and IL-12 or IL-18. **h**, Specific lysis of K562 cells by edited NK cells after 16 h of co-culture with IL-2 and IL-15 at the indicated effector:target ratios. **i**, Specific lysis of K562 cells by untreated healthy donor human NK cells (NT) or cells incubated with 7.5 µg ml⁻¹ methyl-β-cyclodextrin (MβCD) cholesterol for 1 h or 200 µM bovine serum albumin (BSA)-conjugated palmitate or oleate for 24 h after 14 d of expansion with IL-2 and IL-15 at an E:T ratio of 1:2. **j**, Specific lysis of K562 cells by $TRAC^{cRNP}$, $MEF2C^{cRNP}$ NK cells or $MEF2C^{cRNP}$ NK cells pretreated with 200 µM BSA-conjugated oleate for 24 h at an

E:T ratio of 1:2. **k**, Specific lysis of K562 cells at the indicated E:T ratios by healthy control cells, MCHS patient NK cells or MCHS patient NK cells pretreated with 200 µM BSA-conjugated oleate for 24 h after 5 d of expansion with IL-2 and IL-15. **a,d–g**, Gated on CD3⁻CD56⁺ cells. Data are representative of at least two independent experiments. Data represent mean ± s.e.m. or individual paired donors where applicable. Data are representative of $n = 7$ independent donors (**a**), $n = 3$ mice and $n = 6$ independent donors (**b**), $n = 3$ mice (**c**), $n = 6$ independent donors (**d,e**), $n = 3–8$ healthy donors and $n = 2$ patients with MCHS each sampled two independent times (**e,j**), $n = 6$ (**f**), $n = 7$ (**g**), $n = 5$ (**h**) or $n = 6$ (**i**) independent donors. *$P < 0.05$, **$P < 0.01$, ***$P < 0.001$, ****$P < 0.0001$ by two-sided paired t-test or Student's t-test. Specific P values are as follows. For **a**, 0.0060. For **b**, 0.0165. For **c**, 0.0159, <0.0001, 0.0031. For **e**, percent $LDLR^+$ cells, <0.001; MFI, 0.0002. For **f**, day 0, 0.8092; day 5, 0.0464. For **g**, percent IFN-γ⁺ cells, NT (0.9931), IL-18 (0.0147), IL-12 (0.0271); IFN-γ MFI, IL-18 (0·0467). For **h**, 1:4, 0.0045; 1:2, 0.0014; 1:4, 0.0322. For **i**, cholesterol, 0.0036; palmitate, 0.0307; oleate, 0.0460. For **j**, $TRAC^{cRNP}$ versus $MEF2C^{cRNP}$, 0.0191; $MEF2C^{cRNP}$ versus $MEF2C^{cRNP}$ and oleate, 0.0016. For **k**, 1:1, MCHS versus MCHS and oleate, 0.0372; 1:4, healthy control versus MCHS and oleate, 0.0437; 1:4, MCHS versus MCHS and oleate, 0.0229.

signals in other cell types[42], we observed reduced glycolysis in human NK cells following MEF2C loss despite normal S6 kinase phosphorylation, suggesting that S6 kinase activity alone is not sufficient to activate SREBPs in NK cells. Rather, the transcriptional activator activity of MEF2C is likely required in addition to S6 kinase activation for

IL-15-mediated metabolic reprogramming in NK cells. These findings may also point to MEF2C as an alternate mechanism for mTORC1 to activate SREBP signaling in NK cells, supported by studies in other cell types demonstrating that deletion of S6 kinase fails to abrogate SREBP1 activation[43]. STAT5 is also required for cytokine-dependent

induction of MEF2C, suggesting that cooperation between STAT5 and mTOR activity may stimulate metabolic rewiring of activated NK cells, similar to STAT–mTOR crosstalk reported in T cells[44]. Similarly, the mechanisms by which MEF2C activates downstream metabolic pathways are likely complex. As a MEF2 family member, MEF2C relies on a family-conserved MADS DNA-binding domain and an associated MEF2 protein-binding domain to mediate transcriptional regulatory activity[45]. MEF2C may regulate lipid metabolism gene activity either through direct transactivation or the recruitment of additional transcription factors. Sterol species produced by increased SREBP activity can serve as both metabolites and signaling molecules through liver X receptor (LXR) signaling[36]. Thus, the downstream mechanisms of MEF2C-mediated lipid and glucose homeostasis in NK cells are likely multifactorial.

Prior studies have suggested divergent effects of lipid metabolism on NK cell function. Examination of NK cells from patients with obesity indicated that elevated intracellular lipid levels from heightened amounts of circulating fats impair NK cell cytotoxicity via peroxisome proliferator-activated receptor (PPAR)-α- and PPAR-δ-mediated mTOR inhibition[46]. Diffuse large B cell lymphoma-associated NK cells similarly displayed increased lipid levels and corresponding decreased production of IFN-γ, which was recapitulated by ex vivo fatty acid treatment[47]. Conversely, high-cholesterol environments have been proposed to augment the antitumor activity of NK cells in hepatocellular carcinoma by increasing lipid raft formation[48]. While supraphysiologic cellular lipid levels may have beneficial or detrimental effects on NK cell function during obesity or cancer, our findings propose that there is also a minimum requirement for lipid metabolism to adequately support NK cell effector functions after cytokine activation. Our results suggest that the lipid transporter LDLR is required for optimal human NK cell effector function, which is in agreement with studies showing that CD8+ T cells derived from LDLR-deficient mice are similarly impaired in proliferation, cytokine production and cytotoxicity[35]. While we confirm previous results demonstrating that palmitate exposure inhibits cytotoxic NK cell function[46], we find that specific treatment with oleate alone uniquely boosts NK cell cytotoxicity in both WT and MEF2C-deficient NK cells. As SREBP activity is highly sensitive to negative feedback inhibition via insulin-induced gene (INSIG)- and SCAP-mediated repression, lipid supplementation with intermediates such as palmitate rather than end products of lipid metabolic pathways has inhibitory effects on SREBP function in other non-immune cell types, similar to our observations of NK cells[36]. Indeed, previous studies suggest that NK cells treated ex vivo with statins or peripheral NK cells from patients on statin therapy both display defective effector function[49,50]. Because statins inhibit cholesterol synthesis through inhibition of 3-hydroxy-3-methylglutaryl coenzyme A (HMG-CoA) reductase, these findings may reflect an inhibitory buildup of SREBP2 pathway intermediates in statin-treated NK cells that may similarly inhibit NK cell function. Thus, metabolic supplementation with a panel of rationally selected lipids may represent a promising avenue for augmenting MCHS patient NK cells and NK cell adoptive therapy for cancer.

Online content

Any methods, additional references, Nature Portfolio reporting summaries, source data, extended data, supplementary information, acknowledgements, peer review information; details of author contributions and competing interests; and statements of data and code availability are available at https://doi.org/10.1038/s41590-024-01811-2.

References

1. Bjorkstrom, N. K., Strunz, B. & Ljunggren, H. G. Natural killer cells in antiviral immunity. *Nat. Rev. Immunol.* **22**, 112–123 (2022).
2. Mace, E. M. et al. Mutations in *GATA2* cause human NK cell deficiency with specific loss of the CD56^{bright} subset. *Blood* **121**, 2669–2677 (2013).
3. Biron, C. A., Byron, K. S. & Sullivan, J. L. Severe herpesvirus infections in an adolescent without natural killer cells. *N. Engl. J. Med.* **320**, 1731–1735 (1989).
4. Mace, E. M. et al. Biallelic mutations in *IRF8* impair human NK cell maturation and function. *J. Clin. Invest.* **127**, 306–320 (2017).
5. Cottineau, J. et al. Inherited GINS1 deficiency underlies growth retardation along with neutropenia and NK cell deficiency. *J. Clin. Invest.* **127**, 1991–2006 (2017).
6. Gineau, L. et al. Partial MCM4 deficiency in patients with growth retardation, adrenal insufficiency, and natural killer cell deficiency. *J. Clin. Invest.* **122**, 821–832 (2012).
7. Grier, J. T. et al. Human immunodeficiency-causing mutation defines CD16 in spontaneous NK cell cytotoxicity. *J. Clin. Invest.* **122**, 3769–3780 (2012).
8. Cooper, M. A. et al. Human natural killer cells: a unique innate immunoregulatory role for the CD56^{bright} subset. *Blood* **97**, 3146–3151 (2001).
9. Fehniger, T. A. et al. CD56^{bright} natural killer cells are present in human lymph nodes and are activated by T cell-derived IL-2: a potential new link between adaptive and innate immunity. *Blood* **101**, 3052–3057 (2003).
10. Michel, T. et al. Human CD56^{bright} NK cells: an update. *J. Immunol.* **196**, 2923–2931 (2016).
11. Lopez-Verges, S. et al. CD57 defines a functionally distinct population of mature NK cells in the human CD56^{dim}CD16+ NK-cell subset. *Blood* **116**, 3865–3874 (2010).
12. Kee, B. L., Morman, R. E. & Sun, M. Transcriptional regulation of natural killer cell development and maturation. *Adv. Immunol.* **146**, 1–28 (2020).
13. Ramirez, K. et al. Gene deregulation and chronic activation in natural killer cells deficient in the transcription factor ETS1. *Immunity* **36**, 921–932 (2012).
14. Daussy, C. et al. T-bet and Eomes instruct the development of two distinct natural killer cell lineages in the liver and in the bone marrow. *J. Exp. Med.* **211**, 563–577 (2014).
15. Jeevan-Raj, B. et al. The transcription factor Tcf1 contributes to normal NK cell development and function by limiting the expression of granzymes. *Cell Rep.* **20**, 613–626 (2017).
16. Boos, M. D., Yokota, Y., Eberl, G. & Kee, B. L. Mature natural killer cell and lymphoid tissue-inducing cell development requires Id2-mediated suppression of E protein activity. *J. Exp. Med.* **204**, 1119–1130 (2007).
17. Gascoyne, D. M. et al. The basic leucine zipper transcription factor E4BP4 is essential for natural killer cell development. *Nat. Immunol.* **10**, 1118–1124 (2009).
18. Kamizono, S. et al. Nfil3/E4bp4 is required for the development and maturation of NK cells in vivo. *J. Exp. Med.* **206**, 2977–2986 (2009).
19. Holmes, T. D. et al. The transcription factor Bcl11b promotes both canonical and adaptive NK cell differentiation. *Sci. Immunol.* **6**, eabc9801 (2021).
20. Wiedemann, G. M. et al. Deconvoluting global cytokine signaling networks in natural killer cells. *Nat. Immunol.* **22**, 627–638 (2021).
21. Rautela, J., Surgenor, E. & Huntington, N. D. Drug target validation in primary human natural killer cells using CRISPR RNP. *J. Leukoc. Biol.* **108**, 1397–1408 (2020).
22. Riggan, L. et al. CRISPR–Cas9 ribonucleoprotein-mediated genomic editing in mature primary innate immune cells. *Cell Rep.* **31**, 107651 (2020).
23. Collins, P. L. et al. Gene regulatory programs conferring phenotypic identities to human NK cells. *Cell* **176**, 348–360 (2019).
24. Khameneh, H. J. et al. Myc controls NK cell development, IL-15-driven expansion, and translational machinery. *Life Sci. Alliance* **6**, e202302069 (2023).

25. Li, Z. Y. et al. The transcriptional repressor ID2 supports natural killer cell maturation by controlling TCF1 amplitude. *J. Exp. Med.* **218**, e20202032 (2021).

26. van Helden, M. J. et al. Terminal NK cell maturation is controlled by concerted actions of T-bet and Zeb2 and is essential for melanoma rejection. *J. Exp. Med.* **212**, 2015–2025 (2015).

27. Okada, S. et al. Impairment of immunity to *Candida* and *Mycobacterium* in humans with bi-allelic *RORC* mutations. *Science* **349**, 606–613 (2015).

28. Cooley Coleman, J. A. et al. Comprehensive investigation of the phenotype of *MEF2C*-related disorders in human patients: a systematic review. *Am. J. Med. Genet. A* **185**, 3884–3894 (2021).

29. Harrington, A. J. et al. MEF2C hypofunction in neuronal and neuroimmune populations produces MEF2C haploinsufficiency syndrome-like behaviors in mice. *Biol. Psychiatry* **88**, 488–499 (2020).

30. Lin, Q., Schwarz, J., Bucana, C. & Olson, E. N. Control of mouse cardiac morphogenesis and myogenesis by transcription factor MEF2C. *Science* **276**, 1404–1407 (1997).

31. Mitrovic, M. et al. The NK cell response to mouse cytomegalovirus infection affects the level and kinetics of the early CD8^{+} T-cell response. *J. Virol.* **86**, 2165–2175 (2012).

32. Weizman, O. E. et al. ILC1 confer early host protection at initial sites of viral infection. *Cell* **171**, 795–808 (2017).

33. Mah, A. Y. et al. Glycolytic requirement for NK cell cytotoxicity and cytomegalovirus control. *JCI Insight* **2**, e95128 (2017).

34. Marcais, A. et al. The metabolic checkpoint kinase mTOR is essential for IL-15 signaling during the development and activation of NK cells. *Nat. Immunol.* **15**, 749–757 (2014).

35. Bonacina, F. et al. The low-density lipoprotein receptor–mTORC1 axis coordinates CD8^{+} T cell activation. *J. Cell Biol.* **221**, e202202011 (2022).

36. Shimano, H. & Sato, R. SREBP-regulated lipid metabolism: convergent physiology—divergent pathophysiology. *Nat. Rev. Endocrinol.* **13**, 710–730 (2017).

37. Martin-Rufino, J. D. et al. Massively parallel base editing to map variant effects in human hematopoiesis. *Cell* **186**, 2456–2474 (2023).

38. McAuley, G. E. et al. Human T cell generation is restored in CD3δ severe combined immunodeficiency through adenine base editing. *Cell* **186**, 1398–1416 (2023).

39. Cheng, J. et al. Accurate proteome-wide missense variant effect prediction with AlphaMissense. *Science* **381**, eadg7492 (2023).

40. Keating, S. E. et al. Metabolic reprogramming supports IFN-γ production by CD56^{bright} NK cells. *J. Immunol.* **196**, 2552–2560 (2016).

41. Assmann, N. et al. Srebp-controlled glucose metabolism is essential for NK cell functional responses. *Nat. Immunol.* **18**, 1197–1206 (2017).

42. Duvel, K. et al. Activation of a metabolic gene regulatory network downstream of mTOR complex 1. *Mol. Cell* **39**, 171–183 (2010).

43. Lewis, C. A., Griffiths, B., Santos, C. R., Pende, M. & Schulze, A. Genetic ablation of S6-kinase does not prevent processing of SREBP1. *Adv. Enzym. Regul.* **51**, 280–290 (2011).

44. Saleiro, D. & Platanias, L. C. Intersection of mTOR and STAT signaling in immunity. *Trends Immunol.* **36**, 21–29 (2015).

45. Molkentin, J. D., Black, B. L., Martin, J. F. & Olson, E. N. Mutational analysis of the DNA binding, dimerization, and transcriptional activation domains of MEF2C. *Mol. Cell. Biol.* **16**, 2627–2636 (1996).

46. Michelet, X. et al. Metabolic reprogramming of natural killer cells in obesity limits antitumor responses. *Nat. Immunol.* **19**, 1330–1340 (2018).

47. Kobayashi, T. et al. Increased lipid metabolism impairs NK cell function and mediates adaptation to the lymphoma environment. *Blood* **136**, 3004–3017 (2020).

48. Qin, W. H. et al. High serum levels of cholesterol increase antitumor functions of nature killer cells and reduce growth of liver tumors in mice. *Gastroenterology* **158**, 1713–1727 (2020).

49. Tanaka, T., Porter, C. M., Horvath-Arcidiacono, J. A. & Bloom, E. T. Lipophilic statins suppress cytotoxicity by freshly isolated natural killer cells through modulation of granule exocytosis. *Int. Immunol.* **19**, 163–173 (2007).

50. Hillyard, D. Z. et al. Statins inhibit NK cell cytotoxicity by membrane raft depletion rather than inhibition of isoprenylation. *Atherosclerosis* **191**, 319–325 (2007).

Methods

Mice

Mice were bred at UCLA according to animal welfare guidelines of the UCLA Institutional Animal Care and Use Committee. Animal studies were approved by the UCLA Animal Research Committee and the IACUC. Mice were housed in UCLA animal facilities on a 12-h dark–light cycle with ambient temperatures of 20–26 °C and relative humidity of 30–70%. Mice were maintained on commercially available chow (PicoLab Rodent Diet 20, irradiated) and water ad libitum. For all mouse experiments, 8–10-week-old age- and sex-matched littermates were used according to approved institutional protocols. Bone marrow chimeric mice were generated as previously described[51]. Briefly, host mice were lymphodepleted by intraperitoneal (i.p.) injection of busulfan (1 mg ml⁻¹, 25 mg per kg) for 3 consecutive days (total dose of 75 mg per kg). Twenty-four hours after the final busulfan injection, isolated bone marrow from WT, *Mef2c*⁺/⁻ or a 1:1 mixture of WT:*Mef2c*⁺/⁻ bone marrow resuspended in anti-NK1.1 antibody (1 mg ml⁻¹, clone PK136) was transferred by intravenous (i.v.) injection. Bone marrow chimeric mice were allowed to engraft for at least 4 weeks before experimental studies.

Mouse cytomegalovirus infection

MCMV (Smith strain) was serially passaged in BALB/c mice. On the third passage, MCMV viral stocks were prepared by dissociation of salivary glands via dounce homogenization as previously described[52]. In vivo MCMV infection studies were performed by infecting mice with 7.5×10^3 plaque-forming units in 0.5 ml PBS i.p. Mice were monitored and weighed daily and euthanized if body weight decreased >20% from the initial body weight.

Mouse natural killer cell culture

Mouse spleens were collected and dissociated as previously published[52]. NK cells were isolated by negative immunomagnetic selection using the EasySep Mouse NK Cell Isolation Kit (Stemcell). Cytokine and plate-bound antibody stimulation experiments were performed as previously described[51]. For cytokine stimulation, 2×10^4 purified mouse NK cells were cultured for 4 h at 37 °C in CR-10 medium (RPMI 1640 with 25 mM HEPES, 10% FBS, 1% L-glutamine, 1% 200 mM sodium pyruvate, 1% MEM-NEAA, 1% penicillin–streptomycin, 0.5% sodium bicarbonate and 0.01% 55 mM 2-mercaptoethanol) supplemented with brefeldin A (1:1,000, BioLegend), monensin (2 μM, BioLegend), recombinant mouse IL-15 (50 ng ml⁻¹, PeproTech), mouse IL-12 (20 ng ml⁻¹, PeproTech) and/or mouse IL-18 (10 ng ml⁻¹, BioLegend). For plate-bound antibody stimulation, 2×10^4 purified mouse NK cells were stimulated with 4 mg ml⁻¹ precoated antibody to Ly49H (clone RM4-5) for 4 h at 37 °C with recombinant mouse IL-15 (50 ng ml⁻¹, PeproTech), brefeldin A and monensin. For all stimulation experiments, control cells were cultured in CR-10 medium with brefeldin A and monensin alone (NT).

Adoptive transfer of natural killer cells

For whole-splenocyte transfer, 5×10^7 splenocytes were resuspended in PBS and injected i.v. into recipient mice. For transfer of CRISPR cRNP-edited NK cells, NK cells were rested in complete CR-10 medium with mouse IL-15 (50 ng ml⁻¹, PeproTech) for 10 min at 37 °C immediately after CRISPR cRNP electroporation. After resting, congenically distinct cRNP-edited NK cells were mixed at a 1:1 ratio with CD3⁻NK1.1⁺Ly49H⁻KLRG1⁻ cells, resuspended in PBS and injected i.v. into recipient mice. Recipient mice were immediately infected with MCMV by i.p. injection.

Human studies

Fourteen milliliters of peripheral blood was obtained in Vacutainer CPT tubes (BD) from pediatric patients with MCHS at the Greenwood Genetic Center, Greenwood, South Carolina. All blood samples were obtained from patients providing written informed consent according to Greenwood Genetic Center- and UCLA-approved IRB protocols. All patient studies were approved by the ethics committees at Greenwood Genetic Center and UCLA. Participants were not compensated for their participation in the study.

Human natural killer cell culture

Healthy primary human NK cells were isolated and cultured as previously described[51]. Briefly, human PBMCs were obtained either from healthy anonymous donors provided by the UCLA CFAR Virology Core or in Vacutainer CPT tubes (BD) for MCHS patient and healthy control peripheral blood. NK cells were isolated via negative immunoselection using the EasySep Human NK Cell Isolation Kit (Stemcell Technologies). Isolated NK cells were expanded in NK MACS medium (Miltenyi Biotec) supplemented with recombinant human IL-2 (100 IU ml⁻¹, PeproTech) and recombinant human IL-15 (20 ng ml⁻¹, PeproTech) and cultured in 24-well G-Rex plates (Wilson Wolf). Cytokine stimulation assays were performed on cells activated for 15 d with IL-2 and IL-15 or CRISPR cRNP-edited cells on day 6 after CRISPR editing. To stimulate cytokine production, NK cells were cultured in CR-10 medium supplemented with human IL-2 (100 IU ml⁻¹, PeproTech), human IL-15 (20 ng ml⁻¹, PeproTech), K562 human leukemia cells, human IL-12 and/or human IL-18 for 16 h and then analyzed by intracellular flow cytometry. For lipid supplementation studies, NK cells were cultured in NK MACS medium (Miltenyi Biotec) with recombinant human IL-2 (100 IU ml⁻¹, PeproTech), recombinant human IL-15 (20 ng ml⁻¹, PeproTech) and either MβCD cholesterol (7.5 μg ml⁻¹, Sigma), BSA-conjugated palmitate (200 μM, Cayman Chemical) or BSA-conjugated oleate (200 μM, Cayman Chemical).

Guide RNA design

Synthetic sgRNA species were purchased from Synthego. For CRISPR cRNP editing, guide sequences were identified from previously published mouse and human whole-genome CRISPR libraries described previously[53]. For Cas9 base editing, guide sequences were designed based on specific patient point mutations or using SpliceR version 1.2.0 (ref. [54]). The top two to four high-efficiency sgRNA species per target were validated by Sanger sequencing and immunoblotting. Gene targets with indel scores below 20 for all four tested sgRNA species were removed from the final screen. Negative control guides targeting *TRAC* were designed by and purchased directly from Synthego. sgRNA sequences targeting *MEF2C* for cRNP editing are as follows: human *MEF2C*, 5′-GTTGTGGCTGGACACTGGGA-3′; mouse *Mef2c*, 5′-GACAAACTCAGACATTGTGG-3; mouse *Mef2c*, 5′-GAGTTTGTCCGGCTCTCGTG-3′; human *LDLR*, 5′-GCCATCGCAGACCCACTTGT-3′.

CRISPR cRNP editing

cRNP editing of isolated NK cells was performed as previously published[22,52]. cRNP complexes were generated as follows. Synthetic sgRNA (120 pmol, Synthego), Alt-R electroporation enhancer (9 pmol, IDT) and water were added to a 1.5-ml tube per sample. In a separate tube, recombinant SpCas9 (20 pmol, Synthego) was diluted 1:5 with water, and then diluted SpCas9 was added to the sgRNA–enhancer mixture and incubated for 10 min at room temperature to make cRNP complexes. NK cells were electroporated with cRNP complexes using a Neon Transfection system (Thermo Fisher) with a voltage of 1,900 V, a pulse width of 20 ms and one pulse. Electroporated cells were either incubated for 90 min at 37 °C before collection and in vitro culture in complete medium or incubated for 10 min at 37 °C before collection and adoptive transfer in vivo. Gene editing efficiency was evaluated by Sanger sequencing and immunoblotting after 3 d of in vitro culture for mouse NK cells or 6 d for human NK cells.

Cas9 base editing

Synthetic mRNA encoding ABE8e was produced by TriLink Genomics from plasmids provided by the Moriarity laboratory. Base editing of

human NK cells was performed as previously described[54]. Isolated NK cells were electroporated with 5 μg ABE8e mRNA, Alt-R electroporation enhancer (20 pmol, IDT), Protector RNase Inhibitor (diluted 1:5, Roche) and sgRNA (120 pmol, Synthego). Electroporation was performed using a Neon Transfection system (Thermo Fisher) with a voltage of 1,800 V, a pulse width of 10 ms and two pulses. Base-editing efficiency was evaluated by Sanger sequencing after 6 d of in vitro culture. The sgRNA sequence targeting *MEF2C* for base editing is as follows: 5′-TGCTTACCCCAACTGACTGA-3′.

Polymerase chain reaction and Sanger sequencing

PCR and Sanger sequencing to validate CRISPR gene editing was performed as previously published. DNA from isolated NK cells was isolated using the PureLink Genomic mini kit (Thermo Fisher), and DNA concentration was measured using a NanoDrop Eight Spectrophotometer (Thermo Fisher). Fifty nanograms of isolated DNA per sample was amplified by PCR using custom primers surrounding a 500–1,000-bp region targeted by sgRNA species. Sanger sequencing of PCR samples for cRNP-edited or Cas9 base-edited DNA was performed by Azenta, and editing efficiency was analyzed using inference of CRISPR editing (ICE) (Synthego) version 3.0 for cRNP editing or EditR version 1.0.10 for base editing.

Proliferation assays

CTV (Thermo Fisher) stock solution was prepared according to manufacturer protocols and as previously described[52]. Stock CTV solution was diluted 1:10,000 in PBS at 37 °C, and purified human NK cells were labeled for 20 min at 37 °C, protected from light, and then quenched with complete medium for 5 min at 37 °C. Cells were cultured for 6 d in complete NK MACS medium before surface staining and analysis by flow cytometry.

Apoptosis assays

Annexin V and PI staining was performed according to manufacturer protocols (Thermo Fisher, V13242). Briefly, working solutions of FITC annexin V and PI were prepared in 1× annexin binding buffer. Cells were stained in 1:20 diluted stock FITC annexin V and 100 ng PI for 15 min at room temperature, protected from light, before flow cytometry analysis.

Tumor-killing assays

For patient or CRISPR cRNP-edited human NK cells, isolated NK cells were cultured with GFP-expressing K562 cells at the indicated effector-to-target ratios for 16 h at 37 °C in the presence of recombinant human IL-2 (100 IU ml⁻¹, PeproTech) and recombinant human IL-15 (20 ng ml⁻¹, PeproTech). The frequency of remaining viable GFP⁺ cells after co-culture was quantified by flow cytometry. For mouse CRISPR cRNP-edited NK cells, isolated NK cells were cultured with CTV-labeled *B2m*⁻/⁻ MC38 target cells for 16 h at an effector-to-target ratio of 2:1 in the presence of recombinant mouse IL-15 (50 ng ml⁻¹, PeproTech). The frequency of remaining viable CTV⁺ cells after co-culture was quantified by flow cytometry.

Flow cytometry

Single-cell suspensions were stained with fluorophore-conjugated antibodies (BioLegend, Thermo Fisher, eBioscience). Intracellular staining for cytokines was performed using the Cytofix/Cytoperm Fixation/Permeabilization Kit (BD). Intracellular staining for lipids was performed using the eBioscience Foxp3/Transcription Factor staining kit (Thermo Fisher). Intracellular staining for phosphorylated proteins was performed using 4% formaldehyde fixation followed by ice-cold 100% methanol permeabilization and antibody staining following manufacturer recommendations. Flow cytometry was performed using an Attune NxT Acoustic Focusing cytometer (Thermo Fisher). Data were analyzed using FlowJo version 10.7.2 (Tree Star). The following fluorophore-conjugated antibodies were used: human anti-CD3 (1:400, UCHT1), human anti-CD19 (1:100, SJ25-C1), human anti-CD14 (1:100, TuK4), human anti-CD4 (1:100, RPA-T4), human anti-CD8 (1:100, RPA-T8), human anti-CD56 (1:200, TULY56), human anti-CD16 (1:400, CB16), human anti-CD57 (1:100, TB01), human anti-IFN-γ (1:100, B27), human anti-TNF-α (1:100, MAb11), human anti-GzmB (1:100, GB11), human anti-PRF (1:400, B-D48), human anti-CD107a (1:100, H4A3), human anti-LDLR (1:100, C7), human anti-CD25 (1:50, BC96), human anti-CD122 (1:50, TU27), mouse anti-CD45.1 (1:400, A20), mouse anti-CD45.2 (1:400, 104), mouse anti-CD3 (1:100, 17A2), mouse anti-TCR-β (1:100, H57-597), mouse anti-NK1.1 (1:50, PK136), mouse anti-CD27 (1:200, LG.3A10), mouse anti-CD11b (1:200, M1/70), mouse anti-Ly49H (1:600, 3D10), mouse anti-KLRG1 (1:400, 2F1), mouse anti-IFN-γ (1:100, XMG1.2), mouse anti-GzmB (1:100, GB11), mouse anti-CD107a (1:100, 1D4B), mouse anti-CD25 (1:100, PC61), mouse anti-CD122 (1:100, TM-B1), mouse or human anti-phospho-S6 ribosomal protein (1:100, Ser235/Ser236, D57.2.2E), mouse or human anti-phospho-AKT (D9E, 1:100, Ser473), mouse or human anti-phospho-STAT1 (1:50, Tyr701, A-2), mouse or human anti-phospho-STAT5 (1:100, C71E5, Tyr694), mouse or human anti-phospho-STAT5 (1:100, C11C5, Tyr694), Goat Anti-Rabbit IgG H&L FITC (1:100, polyclonal). Staining for neutral lipids was performed using BODIPY 493/503 (500 ng ml⁻¹, Thermo Fisher). Lipid uptake was evaluated by uptake of BODIPY C12 (500 ng ml⁻¹, Thermo Fisher).

Quantitative polymerase chain reaction

For quantitative PCR, RNA was isolated from NK cells using the Quick-RNA Microprep Kit (Zymo). RNA concentration was measured using a NanoDrop Eight Spectrophotometer (Thermo Fisher), and complementary DNA (cDNA) was synthesized using the High-Capacity cDNA Reverse Transcription Kit (Thermo Fisher). Undiluted cDNA was directly assessed in a SYBR Green PCR assay (Applied Biosystems) in a 384-well plate using a LightCycler 480 instrument. Each sample was plated in five technical replicates per PCR primer pair. Primers (*SREBF1*, F (GGAGGGGTAGGGCCAACGGCCT), R (CATGTCTTCGAAAGTGCAATCC); *SCD*, F (TCTAGCTCCTATACCACCACCA), R (TCGTCTCCAACTTATCTCCTCC)) were ordered from IDT (25 mM, standard desalting). Expression was normalized to values from the β-actin housekeeping gene for each sample, and then each experimental sample was normalized to a paired donor control CRISPR cRNP-edited sample for each donor.

Immunoblot analysis

Immunoblots were performed as previously published[51,52]. Cell lysates were prepared in Pierce RIPA buffer (Thermo Fisher) with Halt Protease and Phosphatase Inhibitor (Thermo Fisher). Protein concentration was quantified using the Pierce BCA assay (Thermo Fisher). SDS–PAGE was performed on NuPAGE Novex 4–12% Bis-Tris protein gels (Thermo Fisher) in an XCell II blot module (Thermo Fisher), and samples were transferred to PVDF membranes (MilliporeSigma) and blocked overnight in 5% non-fat dry milk in 1× TBS and 0.1% Tween-20. Proteins of interest were detected using mouse anti-human MEF2C (1:500 dilution, Thermo Fisher, MA5-17119), rabbit anti-human β-actin (1:10,000 dilution, Cell Signaling, CST4970), goat anti-mouse horseradish peroxidase (1:2,000 dilution, Thermo Fisher) and goat anti-rabbit horseradish peroxidase (1:10,000 dilution, Thermo Fisher) antibodies. Proteins were detected with the SuperSignal West Pico PLUS ECL kit (Thermo Fisher) and visualized on an Azure Biosystems c280 imager. Band density was quantified using ImageJ version 1.53t.

Respirometry

Respirometry studies were conducted in a Seahorse XFe96 analyzer. All experiments were conducted at 37 °C and pH 7.4. Rates of oxygen consumption and extracellular acidification of NK cells were measured in medium with 8 mM glucose, 2 mM glutamine, 2 mM pyruvate and 5 mM HEPES. On the day of the experiment, cells were plated at

2.0×10^5 or 2.5×10^5 cells per well in Seahorse XFe96 microplates coated with Cell-Tak at a final concentration of 0.075 mg ml⁻¹. Plates were centrifuged at 500g for 4 min. Respiration was measured in response to oligomycin (2.25 μM), FCCP (two sequential pulses of 0.5 μM) and rotenone (0.2 μM) with antimycin A (1 μM). Respiratory parameters were calculated as previously described[55].

Single-cell metabolic profiling
SCENITH was performed as previously published[52,56]. Briefly, 2.0×10^5 purified human NK cells in complete NK MACS medium were cultured with control (DMSO), 2-deoxyglucose, oligomycin or both 2-deoxyglucose and oligomycin for 4 h at 37 °C together with puromycin. After treatment, cells were stained for surface markers and intracellular staining for puromycin using a custom anti-puromycin antibody provided by the R. Argüello group (Centre National de la Recherge Scientifique (CNRS), France). Metabolic dependencies were calculated based on the geometric MFI of puromycin from inhibitor conditions as published[56].

RNA-seq library construction and sequencing
RNA was isolated from purified NK cells using the Quick-RNA Microprep Kit (Zymo). Ribosomal RNA was depleted from samples using the QIAseq FastSelect -rRNA HMR kit (Qiagen). RNA libraries were prepared according to manufacturer instructions using the Stranded Total RNA Prep Kit (Illumina, 20040525). Libraries were barcoded using IDT for Illumina RNA UD Indexes Set A (Illumina, 20040553), and PCR-amplified libraries were cleaned up using AMPure XP beads (Beckman Coulter). Library quality and concentration were assessed by HSD1000 tape on the 2200 TapeStation (Agilent) and the Qubit 2.0 Fluorometer, and barcoded libraries were pooled at equimolar ratios for sequencing. Sequencing was performed on a NovaSeq 6000 system (Illumina).

RNA-seq analysis
Bulk RNA-seq fastq files were first checked for quality using FastQC (version 0.12.1) and then trimmed to remove low-quality reads and adaptors using Trimmomatic (version 0.40). The parameters used were 'SLIDINGWINDOW:4:20 MINLEN:40 LEADING:3 TRAILING:3'. Next, reads were aligned to either the reference mouse genome (mm10) or the reference human genome (hg38) with STAR (version 2.7.11). STAR was run with default parameters and the '–quantMode gene-Counts' parameter to generate ReadsPerGene.out.tab files, which are tab-delimited files with the raw number of reads mapped to each gene. The unstranded reads (column 2 of ReadsPerGene.out.tab) were combined into one count matrix using Excel. Using DESeq2 (version 1.24.0) with default parameters, differential expression analysis was performed, and the count matrix was normalized. All genes were filtered for significant DEGs by using a threshold of $P < 0.05$. Only genes with counts per million >40 were used for differential expression analysis. The normalized count matrix was used to calculate $\log_2$ (fold change) of DEGs, and heatmaps were generated using the pheatmap package in R based on a |$\log_2$ (fold change)| cutoff of 0.5. Hierarchical clustering was performed using standard parameters in R version 4.3.2. Volcano plots were generated using ggplot2 version 3.4.4. Gene ontology analysis was performed using Gene Ontology and the PANTHER database with the DEGs as input. GSEA was performed using the fgsea package version 3.18 with input genes ranked by $\log_2$ (fold change) $\times$ ($-\log_{10}$ (P value)) and Hallmark human reference pathways h.all.v2023.2 obtained from MSigDB. The Benjamini–Hochberg false discovery rate was used for multiple-comparison correction of pathway analysis.

DICE expression data analysis
Gene expression in human peripheral immune cells sorted by flow cytometry was accessed from the Database of Immune Cell Expression, Expression quantitative trait loci and Epigenomics (DICE) project[57].

Data collection and statistical analyses
For graphs, data are shown as mean ± s.e.m., as paired control and CRISPR cRNP-edited NK cells from the same human donor or mouse or as paired congenically distinct NK cells within the same host animal. No statistical methods were used to predetermine sample sizes, but our sample sizes are similar to those reported in previous publications[22,51,52,58]. Data distribution was assumed to be normal, but this was not formally tested. Experimental groups were not randomized. Data collection and analysis were not performed blind to the conditions of the experiments. Statistical differences were identified using an unpaired two-sided Student's t-test or paired t-test unless otherwise indicated in the figure legend. Kaplan–Meier survival curves were compared using the log-rank (Mantel–Cox) test with correction for testing multiple hypotheses. $P < 0.05$ was deemed significant. Graphs and statistical analyses were generated using GraphPad Prism 10.

Reporting summary
Further information on research design is available in the Nature Portfolio Reporting Summary linked to this article.

Data availability
Sequence data have been deposited in the GEO database under the accession code GSE245463. Gene expression data in sorted human immune cells were provided by the DICE project. Publicly available RNA-seq datasets for human peripheral NK cells sorted by flow cytometry were accessed at GSE112813. Publicly available RNA-seq datasets for cytokine-stimulated NK cells were accessed at GSE140035. RNA-seq data were aligned using the reference mouse genome mm10 or the reference human genome hg38. All other data are available in the main text or Supplementary Information. Source data are provided with this paper.

References
51. Cheng, M. I. et al. The X-linked epigenetic regulator UTX controls NK cell-intrinsic sex differences. *Nat. Immunol.* **24**, 780–791 (2023).
52. Riggan, L. et al. The transcription factor Fli1 restricts the formation of memory precursor NK cells during viral infection. *Nat. Immunol.* **23**, 556–567 (2022).
53. Wang, T. et al. Identification and characterization of essential genes in the human genome. *Science* **350**, 1096–1101 (2015).
54. Kluesner, M. G. et al. CRISPR–Cas9 cytidine and adenosine base editing of splice-sites mediates highly-efficient disruption of proteins in primary and immortalized cells. *Nat. Commun.* **12**, 2437 (2021).
55. Divakaruni, A. S., Paradyse, A., Ferrick, D. A., Murphy, A. N. & Jastroch, M. Analysis and interpretation of microplate-based oxygen consumption and pH data. *Methods Enzymol.* **547**, 309–354 (2014).
56. Arguello, R. J. et al. SCENITH: a flow cytometry-based method to functionally profile energy metabolism with single-cell resolution. *Cell Metab.* **32**, 1063–1075 (2020).
57. Schmiedel, B. J. et al. Impact of genetic polymorphisms on human immune cell gene expression. *Cell* **175**, 1701–1715 (2018).
58. Weizman, O. E. et al. Mouse cytomegalovirus-experienced ILC1s acquire a memory response dependent on the viral glycoprotein m12. *Nat. Immunol.* **20**, 1004–1011 (2019).

Author contributions

J.H.L. designed the project, performed and analyzed all experiments and wrote the paper with input from all authors. A.Z., C.D.L., S.N.S. and Q.F. performed and analyzed experiments. J.H.J. analyzed sequencing data. V.S., S.N.S., E.T.P. and C.G.B. tested sgRNA species and performed the CRISPR cRNP screen. A.B.B. and A.S.D. performed and analyzed Seahorse metabolic experiments. L.R. developed the initial human NK cell culture and CRISPR cRNP system. A.G. and C.W.C. provided $Mef2c^{+/-}$ bone marrow. F.A., J.C.-C. and S.A.S. performed clinical evaluations of patients with MCHS and coordinated and provided patient samples. T.E.O. conceived and designed the project, supervised experiments and wrote the paper.

Competing interests

T.E.O. is a scientific advisor for Modulus Therapeutics and Xyphos Biosciences, companies that have a financial interest in human NK cell-based therapeutics. The Regents of the University of California have filed a provisional patent application with the United States Patent and Trademark Office for using oleate supplementation as a method of augmenting adoptive NK cell therapy. J.H.L. and T.E.O. are listed as inventors on this patent application. The other authors declare no competing interests.

Additional information

Extended data is available for this paper at https://doi.org/10.1038/s41590-024-01811-2.

Supplementary information The online version contains supplementary material available at https://doi.org/10.1038/s41590-024-01811-2.

Correspondence and requests for materials should be addressed to Timothy E. O'Sullivan.

Peer review information *Nature Immunology* thanks the anonymous reviewers for their contribution to the peer review of this work. Primary Handling Editor: N. Bernard, in collaboration with the *Nature Immunology* team.

Reprints and permissions information is available at www.nature.com/reprints.
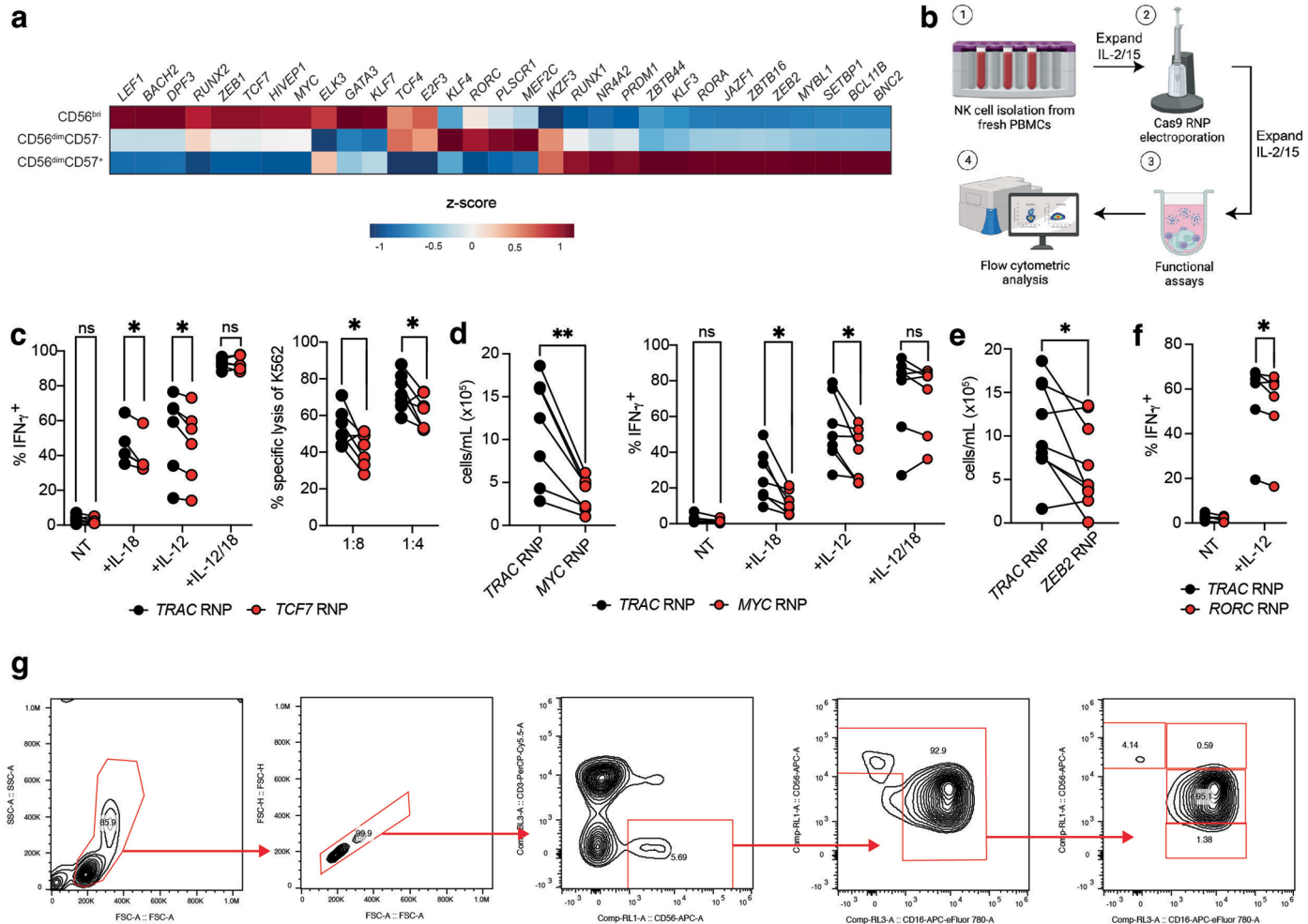
Extended Data Fig. 1 | Functional CRISPR cRNP screen in primary human NK cells identifies positive regulators of human NK cell function.
(**a**) Differentially expressed transcription factors between human NK cell developmental subsets. (**b**) Primary human NK cells are isolated from fresh human PBMCs via negative magnetic bead selection. Following expansion in IL-2/15 for 9 days, cells are electroporated with CRISPR-Cas9 RNP complexes. CRISPR-edited NK cells are further expanded for 6 days before functional and flow cytometric analyses. (**c**) Left, quantification of percent IFN-γ⁺ in $TRAC^{cRNP}$ or $TCF7^{cRNP}$ NK cells after 16 h stimulation with IL-2, IL-15, K562 cells, and IL-12 and/or IL-18. Right, specific lysis of K562 cells after 16 h coculture with IL-2 and IL-15 at indicated effector:target ratios. (**d**) Left, density of viable $TRAC^{cRNP}$ or MYC^{cRNP} NK cells 6 days after cRNP editing expanded with IL-2 and IL-15. Right, quantification

of percent IFN-γ⁺ in $TRAC^{cRNP}$ or MYC^{cRNP} NK cells after 16 h stimulation with IL-2, IL-15, K562 cells, and IL-12 and/or IL-18. (**e**) Density of viable $TRAC^{cRNP}$ or $ZEB2^{cRNP}$ NK cells 6 days after cRNP editing expanded with IL-2 and IL-15. (**f**) Quantification of percent IFN-γ⁺ in $TRAC^{cRNP}$ or $RORC^{cRNP}$ NK cells after 16 h stimulation with IL-2, IL-15, K562 cells, and IL-12 and/or IL-18. (**g**) Representative gating strategy for peripheral human NK cells. Data are representative of n = 6-8 independent donors presented as individual paired donors. *p < 0.05, **p < 0.01 by two-sided paired t test. Specific p-values are as follows: **c** percent IFN-γ⁺ NT = 0.1686, IL-18 = 0.0200, IL-12 = 0.0136, IL-12/18 = 0.8445, % specific lysis 1:8 = 0.0399, 1:4 = 0.0366; **d** cells/mL = 0.0040, percent IFN-γ⁺ NT = 0.0769, IL-18 = 0.0128, IL-12 = 0.0244, IL-12/18 = 0.4241; **e** = 0.0216, **f** = 0.0456.
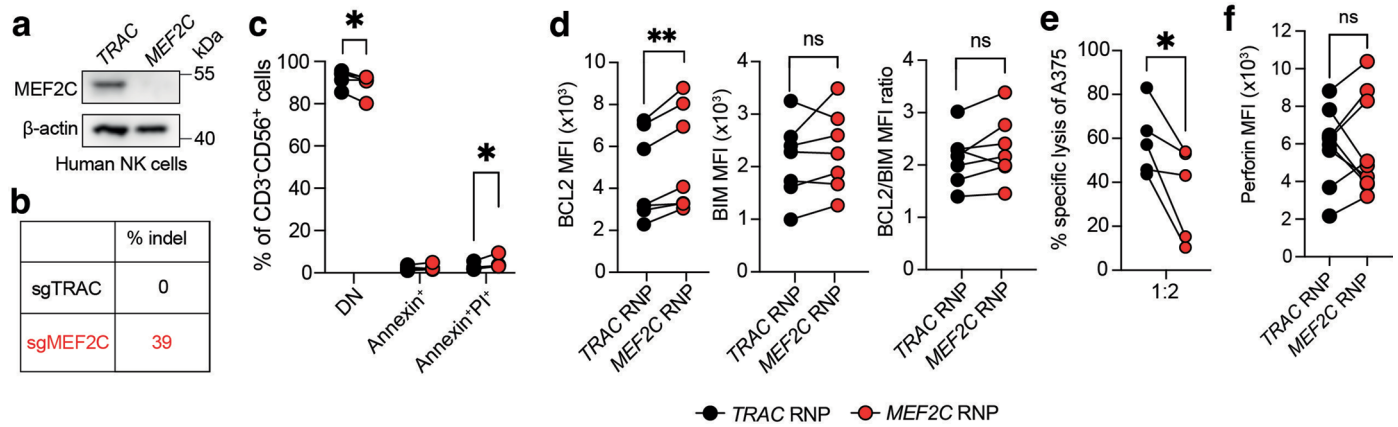
Extended Data Fig. 2 | MEF2C is required for human NK cell function without impacting fitness. (a) Immunoblot showing MEF2C protein expression in *TRAC*cRNP or *MEF2C*cRNP NK cells 6 days after CRISPR cRNP editing. **(b)** Indel percentage by CRISPR cRNP editing in *TRAC*cRNP or *MEF2C*cRNP NK cells 6 days after editing. Sanger sequencing results were analyzed using SYNTHEGO ICE analysis software. **(c)** Quantification of annexin⁺ early apoptotic or annexin⁺PI⁺ late apoptotic *TRAC*cRNP or *MEF2C*cRNP NK cells 6 days after editing. **(d)** MFI of BCL2, BIM, or ratio of BCL2/BIM MFI in *TRAC*cRNP or *MEF2C*cRNP NK cells 6 days after editing. **(e)** Specific lysis of A375 human melanoma cells after 16 h coculture with *TRAC*cRNP or *MEF2C*cRNP NK cells in the presence of IL-2/15. **(f)** MFI of perforin in *TRAC*cRNP or *MEF2C*cRNP NK cells 6 days after editing. Data are representative of n = 4–7 independent donors presented as individual paired donors. *p < 0.05, **p < 0.01 by two-sided paired t test. Specific p-values are as follows: **c** = 0.0361, 0.0204; **d** BCL2 = 0.0047, BIM = 0.2848, BCL2/BIM = 0.1384; **e** = 0.0405; **f** = 0.9390.
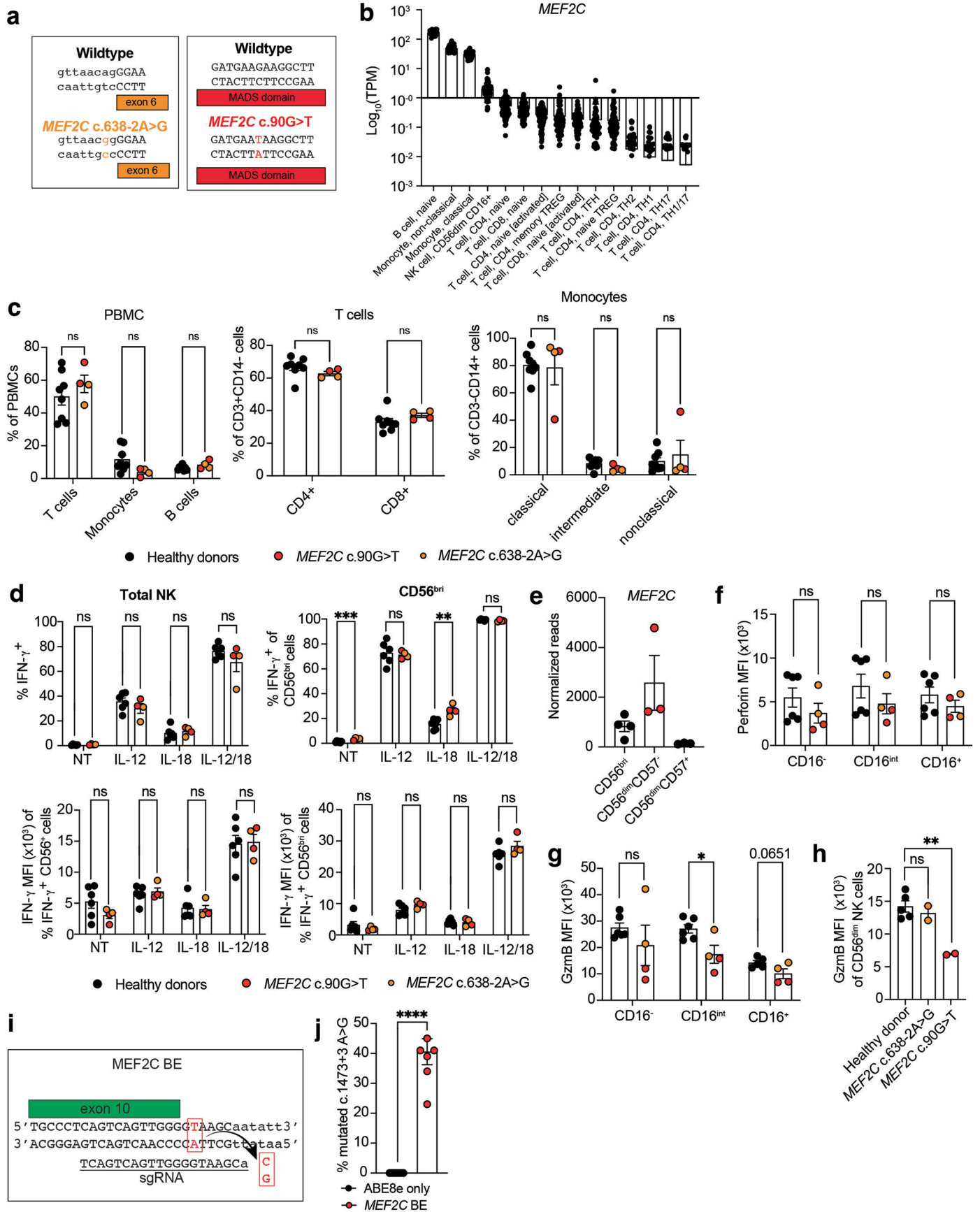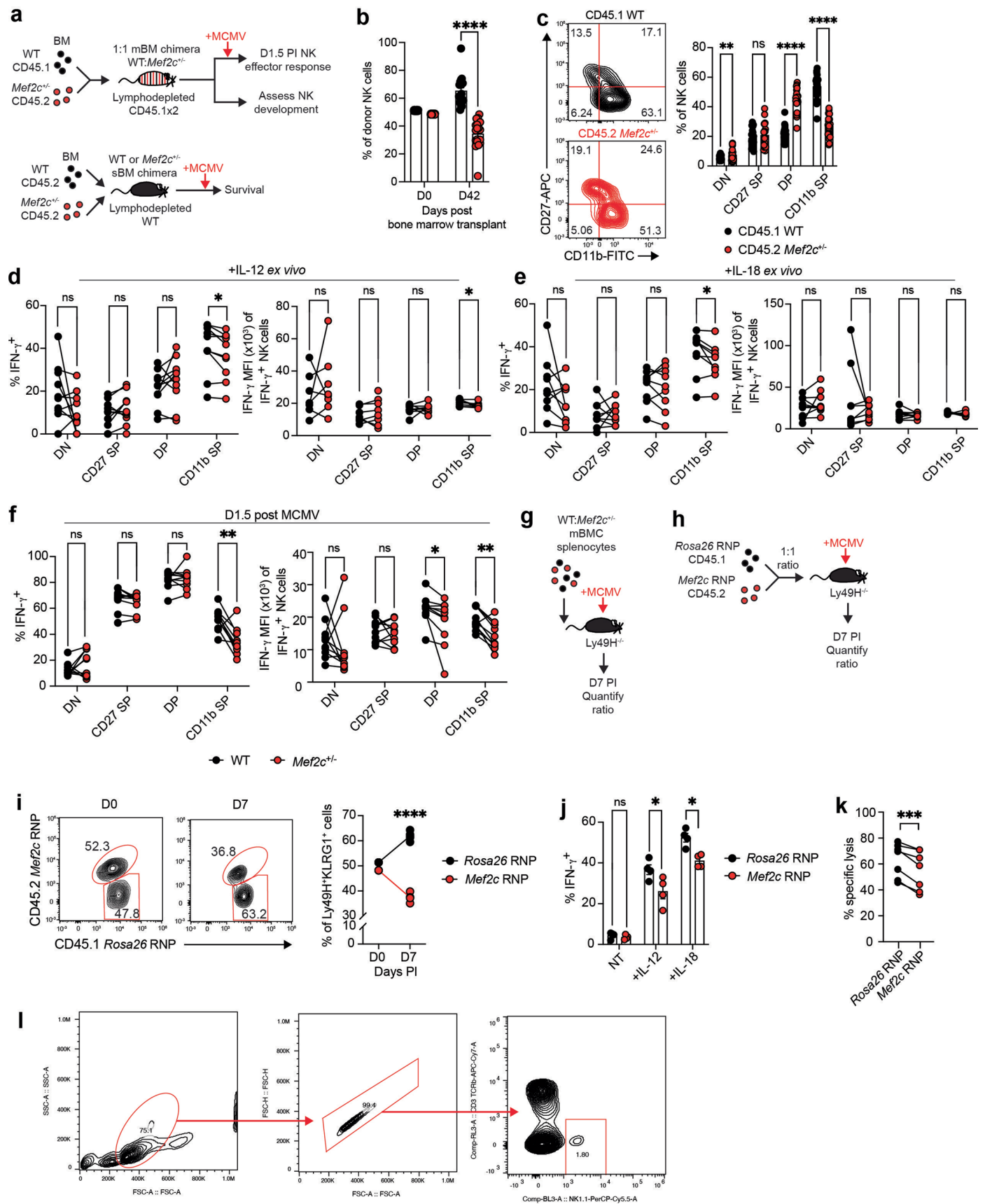
Extended Data Fig. 3 | See next page for caption.

Extended Data Fig. 3 | MEF2C haploinsufficiency disrupts CD56^{dim} NK cells without impacting CD56^{bri} or other circulating immune populations.
(**a**) Schematic of pathogenic point mutations in MCHS patients. (**b**) Expression of MEF2C in FACS-sorted peripheral human immune cells based on DICE database data. (**c**) Frequency of non-NK cell immune populations in peripheral blood of healthy donor control or MCHS patients. (**d**) Percent IFN-γ^{+} (above) and IFN-γ MFI of cytokine-producing cells (below) of total (left) or CD56^{bri} (right) healthy donor control or MCHS patient NK cells stimulated for 16 h with IL-2, IL-15, K562 cells, and IL-12 after 5 d expansion in IL-2/15. (**e**) *MEF2C* transcript expression in NK cell maturation subsets. (**f-g**) MFI of perforin (**f**) or GzmB (**g**) in healthy donor or MCHS patient NK cells by maturation subset. (**h**) MFI of GzmB in healthy donor or MCHS patient CD56^{dim} NK cells. (**i**) Schematic showing adenine base editor (ABE8e) mediated generation of MEF2C point mutation. (**j**) Assessment of point mutation frequency at targeted base using MEF2C-targeting sgRNA in

conjunction with electroporation of ABE8e mRNA in healthy primary human NK cells. Point mutation rate was evaluated by Sanger sequencing and analysis using the EditR package on day 6 post ABE8e electroporation in culture with IL-2/15. (**c**) Left, gated on CD3^{+}CD14^{-} T cells, CD3^{-}CD14^{+} monocytes, and CD3^{-}CD19^{+} B cells. Center, gated on CD3^{+}CD14^{-}CD4^{+} or CD3^{+}CD14^{-}CD8^{+} cells. Right, gated on CD3^{-}CD14^{+}CD16^{hi} classical, CD3^{-}CD14^{+}CD16^{int} intermediate, or CD3^{-}CD14^{+}CD16^{lo} non-classical monocytes. (**d,f-h**) Gated on CD3^{-}CD56^{+} cells or CD3^{-}CD56^{dim}CD16^{+} cells. Data represent mean ± SEM. Data are representative of (**c,d,f-h**) n = 5-8 independent healthy donors alongside n = 2 MCHS patients each sampled two independent times, (**e**) n = 3⁻4 independent donors, or (**j**) n = 6 independent donors. *p < 0.05, **p < 0.01, ***p < 0.001, ****p < 0.0001 by two-sided Student's t test. Specific p-values are as follows: **d** CD56^{bri} percent IFN-γ^{+} NT = 0.0010, IL-18 = 0.0029; **g** = 0.0198; **h** = 0.0039; **j** < 0.0001.
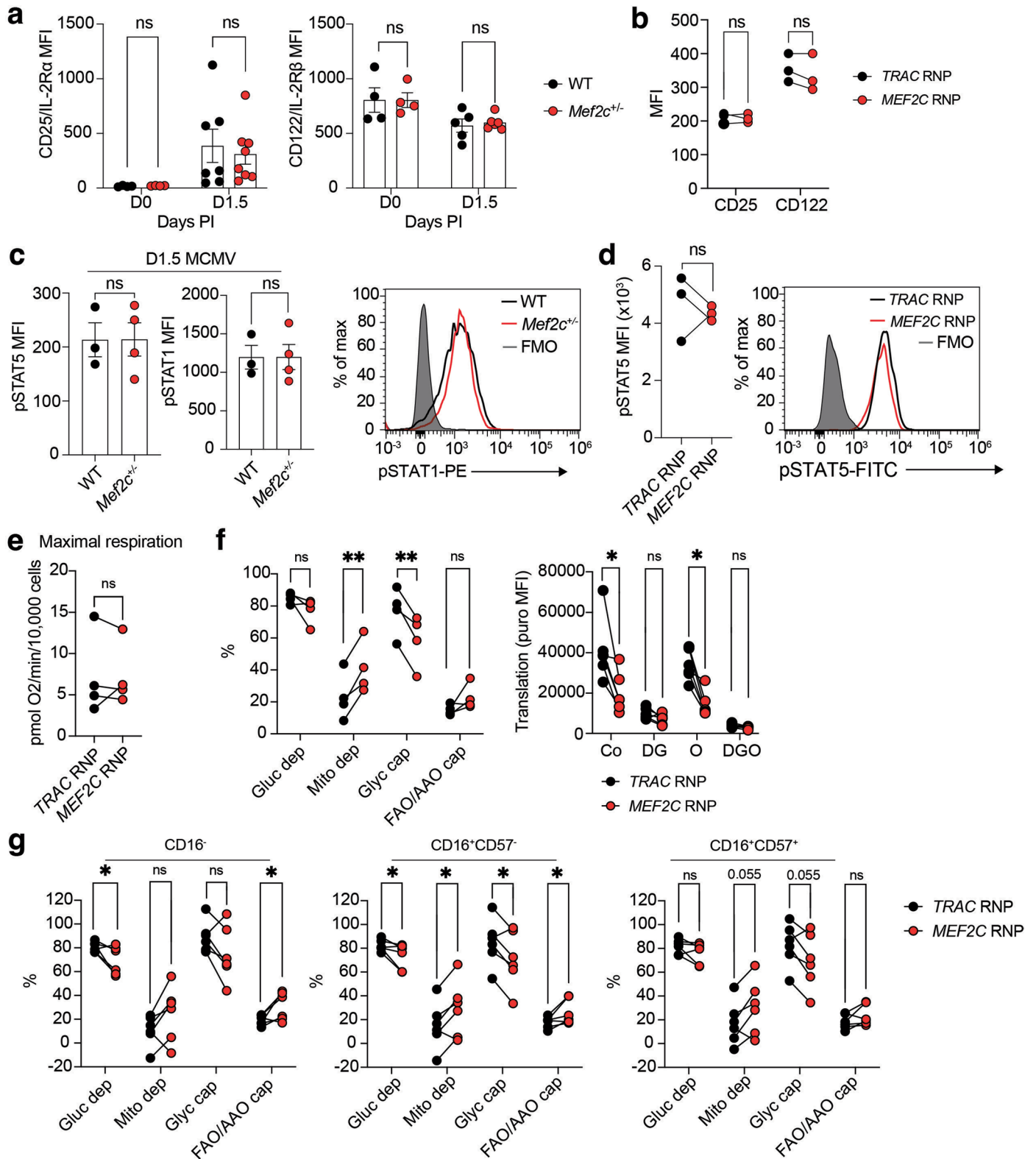
Extended Data Fig. 4 | See next page for caption.

Extended Data Fig. 4 | Mef2c haploinsufficiency impairs antiviral immunity.
(**a**) Schematic of WT:Mef2c$^{+/-}$ mixed bone marrow chimeric (mBMC) mice or
WT and Mef2c$^{+/-}$ single bone marrow chimeric (sBMC) mice. (**b**) Percent WT
or *Mef2c$^{+/-}$* bone marrow-derived NK cells on D0 or D42 post bone marrow
transplant of WT:Mef2c$^{+/-}$ mBMC mice. (**c**) Representative contour plots (left)
and frequencies (right) of peripheral NK cell subsets of wild-type:*Mef2c$^{+/-}$* mixed
bone marrow chimeric (mBMC) mice after 4 weeks engraftment. (**d-e**) Percent
IFN-γ$^+$ (left) and IFN-γ MFI of cytokine-producing cells (right) of splenic NK cells
from WT:Mef2c$^{+/-}$ mBMC mice stimulated *ex vivo* with IL-15 and IL-12 (**d**) or IL-18
(**e**) stratified by maturation subset. (**f**) Percent IFN-γ$^+$ (left) and IFN-γ MFI of
cytokine-producing cells (right) of splenic NK cells from WT:Mef2c$^{+/-}$ mBMC mice
on D1.5 post MCMV. (**g**) Schematic of adoptive transfer of WT:Mef2c$^{+/-}$ mBMC
splenocytes. (**h**) Schematic of adoptive transfer of CRISPR edited *Rosa26*^{cRNP} or
Mef2c^{cRNP} NK cells. (**i**) Representative contour plots (left) and frequency (right) of
Rosa26^{cRNP} or *Mef2c*^{cRNP} Ly49H$^+$KLRG1$^+$ mouse NK cells on D0 and D7 post MCMV.

(**j**) Percent IFN-γ$^+$ of *Rosa26*^{cRNP} or *Mef2c*^{cRNP} NK cells stimulated for 4 h with IL-12 or
IL-18. (**k**) Percent specific lysis of MC38 β2 M$^{-/-}$ by *Rosa26*^{cRNP} or *Mef2c*^{cRNP} NK cells
at 1:1 E:T. (**l**) Representative gating strategy for splenic mouse NK cells. (**b-e,j**)
Gated on CD3$^-$TCRβ$^-$NK1.1$^+$ cells. (**f,i**) Gated on CD3$^-$TCRβ$^-$NK1.1$^+$Ly49H$^+$KLRG1$^+$
cells. Data shown as mean ± SEM, paired WT and *Mef2c$^{+/-}$* NK cells from the same
mBMC mouse, or paired *Rosa26*^{cRNP} and *Mef2c*^{cRNP} NK cells from the same mouse
where applicable. Data representative of at least 2 independent experiments.
Data are representative of (**b,c**) n = 23, (**d,e**) n = 11, (**f**) n = 10, (**i,j**) n = 4, and (**k**) n = 7
mice. *p < 0.05, **p < 0.01, ***p < 0.001, ****p < 0.0001 by two-sided paired t test.
Specific p-values are as follows: **b** < 0.0001; **c** DN = 0.0020, DP < 0.0001, CD11b
SP < 0.0001; **d** CD11b SP percent IFN-γ$^+$ = 0.0144, CD11b SP IFN-γ MFI = 0.0469;
e CD11b SP percent IFN-γ$^+$ = 0.0447; **f** CD11b SP percent IFN-γ$^+$ = 0.0032; DP IFN-γ
MFI = 0.0409, CD11b SP IFN-γ MFI = 0.0016; **i** < 0.0001; **j** IL-12 percent IFN-γ$^+$ =
0.0484, IL-18 percent IFN-γ$^+$ = 0.0466; **k** = 0.0009.

Extended Data Fig. 5 | See next page for caption.

Extended Data Fig. 5 | MEF2C is required for cytokine-activated metabolic reprogramming. (**a**) MFI of CD25/IL-2Rα (left) or CD122/IL-2Rβ (right) of peripheral blood NK cells from WT or $Mef2c^{+/-}$ sBMC mice on D0 or D1.5 of MCMV infection. (**b**) MFI of CD25/IL-2Rα (left) or CD122/IL-2Rβ (right) of $TRAC^{cRNP}$ or $MEF2C^{cRNP}$ human NK cells 6 days post CRISPR edit. (**c**) MFI of pSTAT5 (left) or pSTAT1 (center) and representative histogram of pSTAT1 expression (right) in splenic NK cells from WT or $Mef2c^{+/-}$ sBMC mice on D1.5 of MCMV infection. FMO, fluorescence minus one control. (**d**) MFI of pSTAT5 (left) and representative histogram (right) of $TRAC^{cRNP}$ or $MEF2C^{cRNP}$ human NK cells 6 days post CRISPR edit. FMO, fluorescence minus one control. (**e**) Maximal respiration of $TRAC^{cRNP}$ or $MEF2C^{cRNP}$ human NK cells 6 days post CRISPR edit evaluated by Seahorse extracellular flux assay. (**f**) Metabolic dependencies (left) and translation rate (right) of $TRAC^{cRNP}$ or $MEF2C^{cRNP}$ human NK cells 6 days post CRISPR edit measured by SCENITH. Gluc dep, glucose dependence; Mito dep, mitochondrial dependence; Glyc cap, glycolytic capacity; FAO/AAO cap, fatty acid oxidation/amino acid oxidation capacity; Co, control; DG, 2-deoxyglucose; O, oligomycin. (**g**) Metabolic dependencies of $TRAC^{cRNP}$ or $MEF2C^{cRNP}$ human NK cells 6 days post CRISPR edit measured by SCENITH, stratified by maturation subset. (**a**) Gated on CD3⁻TCRβ⁻NK1.1⁺ cells. (**b,f,g**) Gated on CD3⁻CD56⁺ cells. Data represent (**a**) n = 5-7 mice per group, (**b,d**) n = 3 paired independent donors, (**c**) n = 3-4 mice per group, (**e**) n = 5, or (**f,g**) n = 4-6 paired independent donors. *p < 0.05, **p < 0.01 by two-sided paired t test. Specific p-values are as follows: **f** mito dep = 0.0091, glyc cap = 0.0091, Co puro MFI = 0.0140, O puro MFI = 0.0040; **g** CD16⁻ = 0.0492, 0.0492; CD16⁺CD57⁻ = 0.0491, 0.0322, 0.0322, 0.0491.
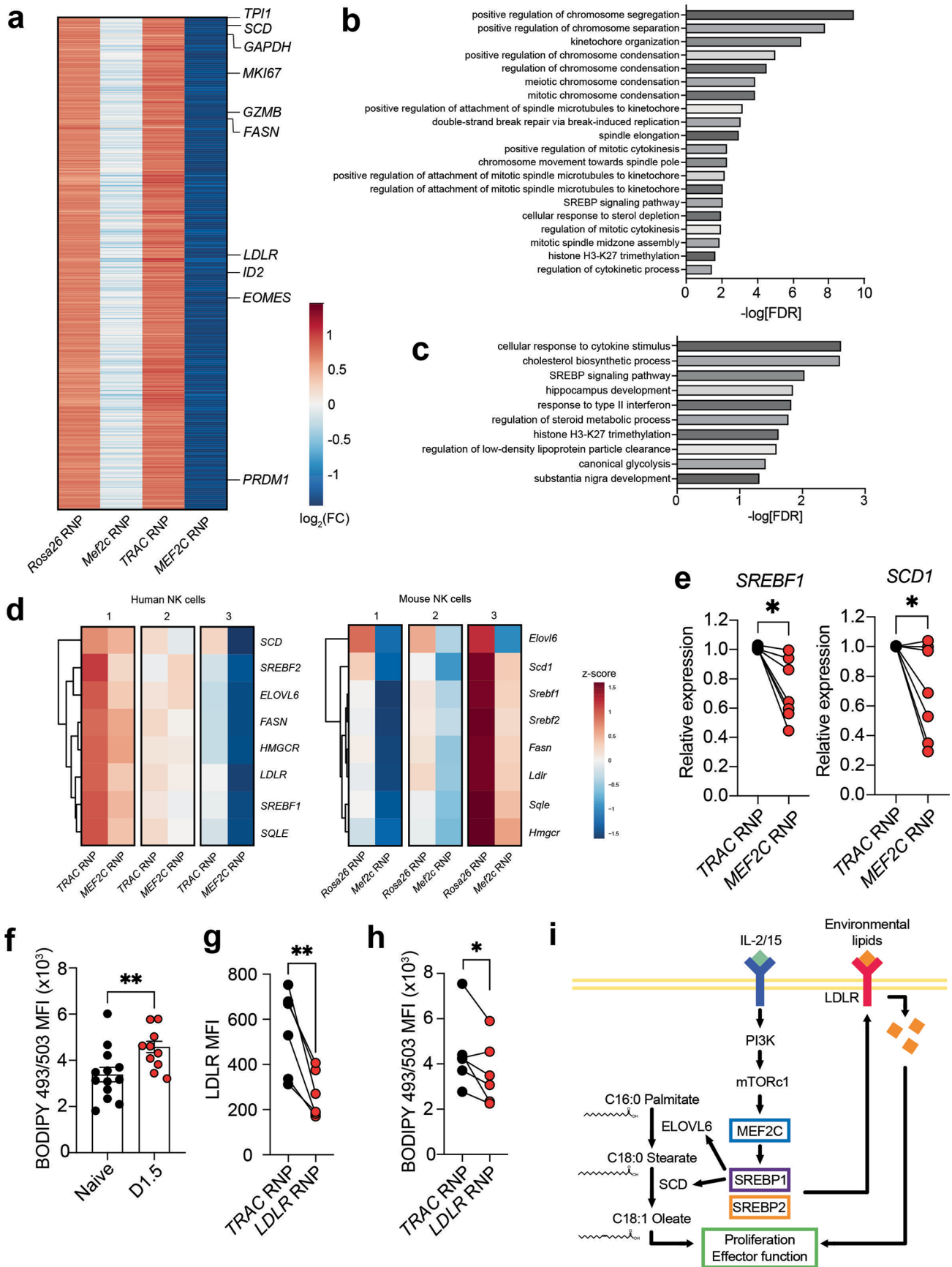
Extended Data Fig. 6 | See next page for caption.

Extended Data Fig. 6 | MEF2C maintains SREBP activity in mouse and human NK cells. (**a**) Heatmap showing differentially expressed genes from RNA-seq performed on human and mouse control and MEF2C knockout NK cells. (**b**) Gene Ontology pathway analysis of downregulated genes conserved between human *MEF2C*^cRNP and mouse *Mef2c*^cRNP NK cells compared to control edited cells ranked by FDR. (**c**) Gene Ontology pathway analysis of downregulated genes conserved between human *MEF2C*^cRNP and mouse *Mef2c*^cRNP NK cells compared to control edited cells ranked by FDR, excluding mitosis and cell division-related pathways. (**d**) Heat maps showing changes in gene expression of canonical SREBP pathway genes separated by biological replicate with hierarchical clustering of genes. (**e**) Transcript expression of *SREBF1* and *SCD1* in *TRAC*^cRNP or *MEF2C*^cRNP human NK cells 6 days post CRISPR edit. (**f**) MFI of BODIPY 493/503 of total splenic NK cells from naive and D1.5 MCMV-infected mice. (**g-h**) MFI of LDLR (**g**) or BODIPY 493/503 (**h**) in *TRAC*^cRNP or *LDLR*^cRNP human NK cells 6 days post CRISPR edit. (**i**) Proposed model of MEF2C-directed lipid metabolic reprogramming driving NK cell effector function in response to cytokine stimulation and mTORc1 activation. Data represent mean ± SEM or individual paired donors where applicable. (**f**) Gated on naïve CD3⁻TCRβ⁻NK1.1⁺ cells or D1.5 CD3⁻TCRβ⁻NK1.1⁺Ly49H⁺KLRG1⁺ cells. (**g-h**) Gated on CD3⁻CD56⁺ cells. Data are representative of (**a-d**) n = 6 mice and n = 3 independent donors, (**e**) n = 6–7 independent donors, (**f**) n = 13 naive and 10 D1.5 mice, or (**g-h**) n = 6 independent donors. *p < 0.05, **p < 0.01 by two-sided paired t test or Student's t test. Specific p-values are as follows: **e** = 0.0108, 0.0421; **f** = 0.0092; **g** = 0.0032, **h** = 0.0485.

nature portfolio

Corresponding author(s):   Timothy O'Sullivan

Last updated by author(s):   Mar 5, 2024

Reporting Summary

Nature Portfolio wishes to improve the reproducibility of the work that we publish. This form provides structure for consistency and transparency in reporting. For further information on Nature Portfolio policies, see our Editorial Policies and the Editorial Policy Checklist.

Statistics

For all statistical analyses, confirm that the following items are present in the figure legend, table legend, main text, or Methods section.

n/a	Confirmed	
☐	☒	The exact sample size (*n*) for each experimental group/condition, given as a discrete number and unit of measurement
☐	☒	A statement on whether measurements were taken from distinct samples or whether the same sample was measured repeatedly
☐	☒	The statistical test(s) used AND whether they are one- or two-sided *Only common tests should be described solely by name; describe more complex techniques in the Methods section.*
☐	☒	A description of all covariates tested
☐	☒	A description of any assumptions or corrections, such as tests of normality and adjustment for multiple comparisons
☐	☒	A full description of the statistical parameters including central tendency (e.g. means) or other basic estimates (e.g. regression coefficient) AND variation (e.g. standard deviation) or associated estimates of uncertainty (e.g. confidence intervals)
☐	☒	For null hypothesis testing, the test statistic (e.g. *F*, *t*, *r*) with confidence intervals, effect sizes, degrees of freedom and *P* value noted *Give P values as exact values whenever suitable.*
☒	☐	For Bayesian analysis, information on the choice of priors and Markov chain Monte Carlo settings
☒	☐	For hierarchical and complex designs, identification of the appropriate level for tests and full reporting of outcomes
☒	☐	Estimates of effect sizes (e.g. Cohen's *d*, Pearson's *r*), indicating how they were calculated

Our web collection on statistics for biologists contains articles on many of the points above.

Software and code

Policy information about availability of computer code

Data collection	Flow Cytometry: Attune NxT Software v3.1.2
Data analysis	Flow cytometry quantification was performed using FlowJo vl0.7.2 (https://www.flowjo.com/solutions/flowjo) Statistical analysis was performed using GraphPad Prism v10 (https://www.graphpad.com/scientific-software/prism) Cas9 base editor sgRNAs were designed using SpliceR v1.2.0. cRNP editing efficiency was analyzed using SYNTHEGO ICE v3.0. Cas9 base editing efficiency was analyzed using EditR v1.0.10. Western blot quantification was performed using ImageJ v.1.53t. Bulk RNA-seq fastq files were first checked for quality using FastQC (version 0.12.1), then trimmed to remove low-quality reads and adaptors using Trimmomatic (version 0.40). The parameters used were SLIDINGWINDOW:4:20 MINLEN:40 LEADING:3 TRAILING:3. Then, reads were aligned to either the reference mouse genome (mm10) or the reference human genome (hg38) with STAR (version 2.7.11). STAR was run with default parameters and the –quantMode geneCounts parameter to generate ReadsPerGene.out.tab files, which are tab-delimited files with the raw number of reads mapped to each gene. The unstranded reads (column 2 of ReadsPerGene.out.tab) were combined into one counts matrix using Excel. Using DESeq2 (version 1.24.0) with default parameters, differential expression analysis was performed, and the counts matrix was normalized. All genes were filtered for significantly differentially expressed genes by $p < 0.05$. Only genes with counts per million (CPM) > 40 were used for differential expression analysis. The normalized counts matrix was used to calculate log2 fold change of differentially expressed genes (DEGs), and heatmaps were generated using the pheatmap package in R based on a |log2 fold change| cutoff of 0.5. Hierarchical clustering was performed using standard parameters in R v4.3.2. Volcano plots were generated using ggplot2 v3.4.4. Gene ontology analysis was performed using Gene Ontology and Panther Database with the DEGs as input. Gene set enrichment analysis was performed using the fgsea package v3.18 with input genes ranked by log2FC*-log10(p-value) and Hallmark human reference pathways

h.all.v2023.2 obtained from MSigDB. The Benjamini-Hochberg false discovery rate (FDR) was used for multiple comparison correction of pathway analysis.

For manuscripts utilizing custom algorithms or software that are central to the research but not yet described in published literature, software must be made available to editors and reviewers. We strongly encourage code deposition in a community repository (e.g. GitHub). See the Nature Portfolio guidelines for submitting code & software for further information.

Data

Policy information about availability of data

All manuscripts must include a data availability statement. This statement should provide the following information, where applicable:
- Accession codes, unique identifiers, or web links for publicly available datasets
- A description of any restrictions on data availability
- For clinical datasets or third party data, please ensure that the statement adheres to our policy

Sequencing data are accessible from the GEO database under GSE245463. Gene expression data in sorted human immune cells was provided by the Database of Immune Cell Expression, Expression quantitative trait loci (eQTLs) and Epigenomics (DICE) Project. Publicly available RNA sequencing datasets for FACS-sorted human peripheral NK cells were accessed at GSE112813. Publicly available RNA sequencing datasets for cytokine-stimulated NK cells were accessed at GSE140035. RNA sequencing was aligned using reference mouse genome mm10 or reference human genome hg38. All other data are available in the main text or supplementary materials.

Research involving human participants, their data, or biological material

Policy information about studies with human participants or human data. See also policy information about sex, gender (identity/presentation), and sexual orientation and race, ethnicity and racism.

Reporting on sex and gender	Sex and gender were not considered in study design among human subjects in the present study. The findings we present are applicable to both male and female sex. Patient sex was based on assigned sex at birth. Patient gender was not noted in the study. Patient sex data can be found in Table 1.
Reporting on race, ethnicity, or other socially relevant groupings	Human subjects in the present study were not categorized by socially constructed variables as recruitment was based solely on MEF2C mutation status.
Population characteristics	Patient 1 is a 4 year old male diagnosed with a pathogenic MEF2C point mutation c.638-2A>G. He displays absent speech, global developmental delay, facial dysmorphism, and social abnormalities as well as autism spectrum disorder. Medication use includes cyproheptadine, levatiracetam, diazepam, and atropine. Patient 2 is an 8.5 year old female diagnosed with a pathogenic MEF2C abnormality at c.90G>T. She is developmentally delayed and displays seizures, absent speech, hypotonia, facial dysmorphisms, and social abnormalities. On imaging, patient 2 has presented previously with brain MRI abnormalities involving the hippocampi and left lateral ventricle. Patient 2 is currently taking oxcarbazepine, levatiracetam, leuprorelin, midazolam, and vitamins. All patients provided written informed consent according to local ethics committees and based on Greenwood Genetic Center and UCLA IRB-approved protocols.
Recruitment	Patients were recruited to the study by Greenwood Genetic Center staff. Patients had previously been seen at Greenwood Genetic Center and were directly contacted. All patients provided written informed consent according to local ethics committees and based on Greenwood Genetic Center and UCLA IRB-approved protocols. Potential biases were minimized by having patient recruitment performed by clinical staff rather than the study researchers. While selection bias may skew the study participant pool toward those clinically presenting with immune phenotypes, our study cohort displays a range of mild to severe immune sequelae suggesting bias had minimal impact.
Ethics oversight	Study protocols were approved by ethics committees of Greenwood Genetic Center and UCLA IRBs.

Note that full information on the approval of the study protocol must also be provided in the manuscript.

Field-specific reporting

Please select the one below that is the best fit for your research. If you are not sure, read the appropriate sections before making your selection.

☒ Life sciences ☐ Behavioural & social sciences ☐ Ecological, evolutionary & environmental sciences

For a reference copy of the document with all sections, see nature.com/documents/nr-reporting-summary-flat.pdf

Life sciences study design

All studies must disclose on these points even when the disclosure is negative.

Sample size	A suitable sample size was chosen based on our previous studies to ensure adequate reproducibility of results. Sample sizes were chosen based on previously published experiments. CHeng MI, Li JH, Riggan L, Chen B, Tafti RY, Chin S, Ma F, Pellegrini M, Hrncir H, Arnold AP, O'Sullivan TE, Su MA. The X-linked epigenetic regulator UTX controls NK cell-intrinsic sex differences. Nature Immunology (2023).

Riggan L, Ma F, Li JH, Fernandez E, Nathanson DA, Pellegrini M, O'Sullivan TE. Fli1 restricts the formation of memory precursor NK cells during viral infection. Nature Immunology (2022)

Riggan, L., Hildreth, A.D., Rolot, M., Wong Y.Y., Satyadi, W., Sun, R., Huerta, C., and O'Sullivan, T.E. CRISPR Cas9 ribonucleoprotein-mediated genomic editing in primary mature innate immune cells. Cell Reports (2020)

Orr-El Weizman, Eric Song, Nicholas M. Adams, Andrew D. Hildreth, Luke Riggan, Chirag Krishna, Oscar A. Aguilar, Christina S. Leslie, James R. Carlyle, Joseph C. Sun , and Timothy E. O'Sullivan. Mouse cytomegalovirus-experienced ILC1s acquire a memory response dependent on the viral glycoprotein m12. Nature Immunology (2019)

Sample size for mouse experiments was at least 3 per group.

Data exclusions	None
Replication	Experimental findings were reproducible across multiple experiments. Experiments were repeated independently 2-3 times.
Randomization	Experimental groups in mouse experiments were not randomized. Age-matched and sex-matched mice were used for our experiments. Experimental samples in non-animal experiments were not randomized as we were studying properties of genetically defined groups.
Blinding	Experiments were not performed in a blinded fashion. Blinding was not relevant to our study, since we are studying and comparing the property of known cell types.

Reporting for specific materials, systems and methods

We require information from authors about some types of materials, experimental systems and methods used in many studies. Here, indicate whether each material, system or method listed is relevant to your study. If you are not sure if a list item applies to your research, read the appropriate section before selecting a response.

Materials & experimental systems

n/a	Involved in the study
☐	☒ Antibodies
☐	☒ Eukaryotic cell lines
☒	☐ Palaeontology and archaeology
☐	☒ Animals and other organisms
☒	☐ Clinical data
☒	☐ Dual use research of concern
☒	☐ Plants

Methods

n/a	Involved in the study
☒	☐ ChIP-seq
☐	☒ Flow cytometry
☒	☐ MRI-based neuroimaging

Antibodies

Antibodies used:
human CD3 (UCHT1) PerCP/Cy5.5 1:400 Biolegend #300429
human CD19 (SJ25-C1) FITC 1:100 Thermo Fisher #MHCD1901
human CD14 (TuK4) APC 1:100 Thermo Fisher #MHCD1405
human CD4 (RPA-T4) AlexaFluor 700 1:100 Biolegend #300526
human CD8 (RPA-T8) Pacific Blue 1:100 Biolegend #301026
human CD56 (TULY56) PE 1:200 Thermo Fisher #12-0566-42
human CD16 (CB16) APC-eFluor 780 1:400 Thermo Fisher #12-0168-42
human CD57 HNK-1 PE/Cy7 1:100 Biolegend #359623
human IFN-γ (B27) PE 1:100 Biolegend #506506
human TNF-a (MAb11) PE/Cy7 1:100 Biolegend #502929
human GzmB (GB11) FITC 1:100 Biolegend #515403
human PRF (B-D48) Pacific Blue 1:400 Biolegend #353305
human CD107a (H4A3) PE 1:100 Biolegend #328607
human LDLR (C7) PE 1:100 BD #565653
human CD25 (BC96) BV510 1:50 Biolegend #302639
human CD122 (TU27) PerCP/eFluor 710 1:50 eBioscience 46-1228-41
mouse/human pS6 (D57.2.2E) 1:100 Cell Signaling CST4858
mouse/human pAKT (D9E) 1:100 Cell Signaling CST4060
mouse/human pSTAT5 (C71E5) PE 1:100 Cell Signaling CST5387S
mouse/human pSTAT5 (C11C5) 1:100 Cell Signaling CST9359T
mouse/human phospho-STAT1 1:50 (Tyr701) (A-2)
Goat anti-rabbit H&L (Polyclonal - ab6717) FITC 1:200 Abcam #ab6717
mouse CD45.1 (A20) PE/Cy7 1:400 Biolegend #110729
mouse CD45.2 (104) AlexaFluor 700 1:400 Biolegend #109821
mouse NK1.1 (PK136) Percp/Cy5.5 1:50 Biolegend #108728
mouse TCRβ (H57-597) APC/Cy7 1:100 Biolegend #109220
mouse CD3 (17A2) APC/Cy7 1:100 Biolegend #100222
mouse Ly49H (3D10) Alexa Fluor 647 1:600 Biolegend #144710
mouse IFN-γ (XMG1.2) PE 1:100 Biolegend #505807
mouse CD27 (LG.3A10) APC 1:200 Biolegend #124211

mouse CD11b (M1/70) AlexaFluor 700 1:200 Biolegend #101222
mouse KLRG1 (2F1) PE 1:400 Biolegend #138407
mouse GzmB (GB11) FITC 1:100 Biolegend #515403
mouse CD107a (1D4B) PE 1:100 Biolegend #121611
mouse CD25 (PC61) PE 1:100 Biolegend #102007
mouse CD122 (TM-B1) FITC 1:100 #123207
mouse anti-human MEF2C (1:500 dilution, Thermo Fisher #MA5-17119)
rabbit anti-human B-actin (1:10,000 dilution; Cell Signaling CST4970)
goat anti-mouse horseradish peroxidase (1:2,000 dilution, Thermo Fisher)
goat anti-rabbit horseradish peroxidase (1:10,000 dilution, Thermo Fisher)

Validation

The antibody validation is provided on the supplier website. All antibodies were validated with proper isotype controls using primary mouse or human lymphocytes.

Supplier validation from Biolegend was described as follows: Specificity testing of 1-3 target cell types with either single- or multi-color analysis (including positive and negative cell types). Once specificity is confirmed, each new lot must perform with similar intensity to the in-date reference lot. Brightness (MFI) is evaluated from both positive and negative populations. Each lot product is validated by QC testing with a series of titration dilutions.

Supplier validation from Thermo Fisher was described as follows: antibody has been pre-titrated and tested by flow cytometric analysis of normal human peripheral blood cells.

Supplier validation from Abcam was described as follows: We include relevant controls, routinely running unstained, positive, negative, isotype, viability, Fc-blocking, fluorescence minus one (FMO), and single-staining controls. For an FMO control, we stain all our samples with fluorescent conjugates except the one that is being tested. This shows the contribution of the other fluorescent conjugates in the signal of the unlabeled channel. This control is important for determining non-specific binding of an antibody.

Supplier validation from Cell Signaling was described as follows: CST scientists test all our products in relevant applications such as western blotting, immunoprecipitation, immunofluorescence, immunohistochemistry, flow cytometry, and chromatin immunoprecipitation. When an antibody is recommend for a particular application, it indicates that the antibody has passed rigorous application-specific testing standards. Additionally, our scientists create specialized (optimized) immunostaining protocols for individual products, saving you time and reagents. We routinely test our antibodies on multiple species including human, monkey, mouse, and rat.

Eukaryotic cell lines

Policy information about cell lines and Sex and Gender in Research

Cell line source(s)

MC38 B2M KO cells were derived in the lab of Dr. Antoni Ribas, MD, PhD. The MC38 cell line was originally generated at the NCI Surgery Branch (originally labeled as Colo38), and was obtained from Dr. Robert Prins (Department of Neurosurgery, UCLA).

K562 cells were obtained from ATCC (CCL-243).

Authentication

Cell lines were not authenticated before use.

Mycoplasma contamination

Cell lines were tested negative for mycoplasma before use using MycoAlert Mycoplasma Detection Kit (Lonza).

Commonly misidentified lines
(See ICLAC register)

No commonly misidentified cell lines were used in this study.

Animals and other research organisms

Policy information about studies involving animals; ARRIVE guidelines recommended for reporting animal research, and Sex and Gender in Research

Laboratory animals

The following mouse strains were used in this study: C57BL/6 (CD45.2+) (Jackson Labs, #000664), B6.SJL (CD45.1+) (Jackson Labs, #002114), Mef2c-het mice were provided by the Cowan Lab (Department of Neuroscience, MUSC). As described in Harrington et al Biol Psychiatry 2020, Mef2c-het mice were generated by crossing Mef2c-flox mice (RRID:MGI:3719006) to Prm-Cre mice (The Jackson Laboratory, Bar Harbor, ME). The Prm-Cre allele was subsequently removed during repeated backcrossing to C57BL/6J wild-type mice. All experiments used 8-10 week old age- and sex-matched mice.

Mice were housed in UCLA animal facilities on a 12 hour dark/light cycle with ambient temperatures of 20-26C and relative humidity of 30-70%.

Wild animals

No wild animals were used in this study.

Reporting on sex

Both male and female mice were used for all studies to account for sex-specific effects. Data are presented as aggregated male and female animals.

Field-collected samples

No field-collected samples were used.

Ethics oversight	Mice were bred at UCLA in accordance of the Institutional Animal Care and Use Committee (IACUC). Animal studies were approved by the UCLA Animal Research Committee and IACUC.

Note that full information on the approval of the study protocol must also be provided in the manuscript.

Plants

Seed stocks	N/A
Novel plant genotypes	N/A
Authentication	N/A

Flow Cytometry

Plots

Confirm that:

☒ The axis labels state the marker and fluorochrome used (e.g. CD4-FITC).

☒ The axis scales are clearly visible. Include numbers along axes only for bottom left plot of group (a 'group' is an analysis of identical markers).

☒ All plots are contour plots with outliers or pseudocolor plots.

☒ A numerical value for number of cells or percentage (with statistics) is provided.

Methodology

Sample preparation	Spleens were dissociated by mashing using a plunger from a 1 ml syringe through a 40 uM filter into complete media. To isolate lymphocytes from liver, the tissues were physically dissociated using a glass tissue homogenizer and purified using 40% Percoll. Lung lymphocytes were incubated with Collagenase D and then filtered into a single cell suspension. Bone marrow isolated by a mortar and pestle. Red blood cells in all tissues were lysed using ACK lysis buffer. Human peripheral blood samples were collected in BD Vacutainer CPT tubes. After blood collection, CPT tubes were centrifuged for 30 min at 1800 RCF then inverted to resuspend the buffy coat into plasma. Lymphocytes were removed from the top layer, centrifuged for 5 min at 1200 RPM, and resuspended in complete RPMI.
Instrument	Attune NxT Acoustic Focusing Cytometer
Software	Attune NxT Software v3.1.2, with quantification performed using FlowJo v10.7.2
Cell population abundance	NK cell abundance was determined by flow cytometry after purification or within homogenized tissues. Human NK cell purity from fresh PBMCs post-isolation was >85% CD3-CD56+ NK cells. Mouse NK cell purity post-isolation was >90% CD3/TCRb-NK1.1+ NK cells. Mouse NK cell abundance within peripheral tissues ranged from 1-5%.
Gating strategy	Mouse NK cell = CD3,TCRb- NK1.1+ Human NK cell = CD3-CD56+ Viable lymphocytes were identifed by FSC/SSC at approximately FSC 400K/SSC 150K-600K based on FSC voltage 190/SSC voltage 380. For IFN-y and CD107a positive populations, the boundary between positive and negative populations was determined based on the upper boundary of IFN-y or CD107a expression in unstimulated control cells.

☒ Tick this box to confirm that a figure exemplifying the gating strategy is provided in the Supplementary Information.